186795.v1

Revised: 03/08/2013

Original paper

*J. **Oxidative Medicine and Cellular Longevity** (Hindawi Publishing Co.)*

http://mts.hindawi.com/author/submit/journals/oximed/joss/

Adaptive Redox Response of Mesenchymal Stromal Cells to Stimulation with Lipopolysaccharide Inflammagen: Mechanisms of Remodeling of Tissue Barriers in Sepsis

Nikolai V. Gorbunov[1*], Bradley R. Garrison[1], Dennis P. McDaniel[2], Min Zhai[1], Pei-Jyun Liao[1], Dilber Nurmemet[1], and Juliann G. Kiang[1,3,4*]

[1]Armed Forces Radiobiology Research Institute, [2]Big Instrumentation Center, [3]Department of Medicine, [4]Department of Radiation Biology, Uniformed Services University of the Health Sciences, Bethesda, Maryland

[*]**The corresponding authors NVG and JGK equally contributed to the presented work.**

Report Documentation Page

Form Approved
OMB No. 0704-0188

1. REPORT DATE	2. REPORT TYPE	3. DATES COVERED
08 MAR 2013		**00-00-2013 to 00-00-2013**

4. TITLE AND SUBTITLE	5a. CONTRACT NUMBER
Adaptive Redox Response of Mesenchymal Stromal Cells to Stimulation with Lipopolysaccharide Inflammagen: Mechanisms of Remodeling of Tissue Barriers in Sepsis	5b. GRANT NUMBER
	5c. PROGRAM ELEMENT NUMBER
6. AUTHOR(S)	5d. PROJECT NUMBER
	5e. TASK NUMBER
	5f. WORK UNIT NUMBER
7. PERFORMING ORGANIZATION NAME(S) AND ADDRESS(ES) **Armed Forces Radiobiology Research Institute,Uniformed Services University of the Health Sciences,Bethesda,MD,20814**	8. PERFORMING ORGANIZATION REPORT NUMBER
9. SPONSORING/MONITORING AGENCY NAME(S) AND ADDRESS(ES)	10. SPONSOR/MONITOR'S ACRONYM(S)
	11. SPONSOR/MONITOR'S REPORT NUMBER(S)

12. DISTRIBUTION/AVAILABILITY STATEMENT
Approved for public release; distribution unlimited

13. SUPPLEMENTARY NOTES
Preprint, J. Oxidative Medicine and Cellular Longevity, 2013

14. ABSTRACT

Acute bacterial inflammation is accompanied by excessive production of reactive oxygen and nitrogen species (ROS and RNS), which ultimately results in redox-stress, a leading pathogenic factor of the septic multiple organ dysfunction syndromes. According to the current paradigm, the inflammatory redox-stress is primarily attributed to the defense responses of the reticuloendothelial, endothelial, and lymphoepithelial components of tissue barriers to infections. Meanwhile, a large body of data accumulated in the last decade has pointed to an emerging role of ubiquitous mesenchymal stromal cells (MSCs) playing in the antibacterial and inflammatory events. In conjunction with this evidence, investigation of cellular pathways up-regulated in MSCs under redox stress conditions may provide new insights into mechanisms driving homeostatic responses of defense barriers to infections. This report presents results of in vitro investigations of the redox response of mouse MSCs to stimulation with Lipopolysaccharide (LPS) inflammagen. We have shown that MSCs treated with LPS experienced redox-stress due to induction of nitric oxide synthase (iNOS) and release of RNS and ROS. The compensatory response of MSCs to the LPS-induced cytotoxic stress was associated with activation of a number of the adaptive redox-response elements such as NFkB, Ref1, TRX1, Nrf2 and HO1, and autophagy, a cellular homeostatic process of remodeling and turnover of compromised cellular constituents. We propose that the cell survival mechanisms activated in LPS-treated MSCs in vitro could be a part of adaptive responses employed by stromal cells under septic conditions.

15. SUBJECT TERMS

16. SECURITY CLASSIFICATION OF:			17. LIMITATION OF ABSTRACT	18. NUMBER OF PAGES	19a. NAME OF RESPONSIBLE PERSON
a. REPORT **unclassified**	b. ABSTRACT **unclassified**	c. THIS PAGE **unclassified**	**Same as Report (SAR)**	**45**	

Standard Form 298 (Rev. 8-98)
Prescribed by ANSI Std Z39-18

Abstract

Acute bacterial inflammation is accompanied by excessive production of reactive oxygen and nitrogen species (ROS and RNS), which ultimately results in redox-stress, a leading pathogenic factor of the septic multiple organ dysfunction syndromes. According to the current paradigm, the inflammatory redox-stress is primarily attributed to the defense responses of the reticuloendothelial, endothelial, and lymphoepithelial components of tissue barriers to infections. Meanwhile, a large body of data accumulated in the last decade has pointed to an emerging role of ubiquitous mesenchymal stromal cells (MSCs) playing in the antibacterial and inflammatory events. In conjunction with this evidence, investigation of cellular pathways up-regulated in MSCs under redox stress conditions may provide new insights into mechanisms driving homeostatic responses of defense barriers to infections. This report presents results of *in vitro* investigations of the redox response of mouse MSCs to stimulation with *Lipopolysaccharide* (LPS) inflammagen. We have shown that MSCs treated with LPS experienced redox-stress due to induction of nitric oxide synthase (iNOS) and release of RNS and ROS. The compensatory response of MSCs to the LPS-induced cytotoxic stress was associated with activation of a number of the adaptive redox-response elements such as NFkB, Ref1, TRX1, Nrf2 and HO1, and autophagy, a cellular homeostatic process of remodeling and turnover of compromised cellular constituents. We propose that the cell survival mechanisms activated in LPS-treated MSCs *in vitro* could be a part of adaptive responses employed by stromal cells under septic conditions.

1 Introduction

It is well documented that common complications of traumatic injury and acute irradiation syndrome are bacterial infection and associated sepsis, which are considered as the major factors of high morbidity and mortality of the illnesses [1-4]. Sepsis has been defined as the acute systemic inflammatory response syndrome that occurs during infection and toxicosis [2]. Therefore, work in the field of septic shock has long focused on inflammation as the leading pathogenic mechanism. However, a variety of therapeutic approaches, mainly anti-inflammatory in nature, have mostly failed to cure human sepsis (*e.g.,* studies involving IL-1α, TNF-β, prostaglandins, leukotrienes *etc*.) [2, 5]. Due to the failure of anti-inflammatory strategies, the physician community was faced with the question of whether inflammation or immunosuppression is the driving factor of death from sepsis [2, 5]. This problem leads to the searching for other potential mechanisms that could produce adverse effects on host metabolome resulting in septic toxicosis. The elucidation of other major (vital) pathways affected by the oxidative stress (redox stress) from the acute bacterial inflammation is critical to solving this problem. Indeed, cumulative oxidative effects of reactive oxygen and nitrogen species (ROS and RNS, respectively) generated in over-reactive responses of the reticuloendothelial, endothelial, and lymphoepithelial cells to bacteria and bacterial factors, can eventually alter integrity of tissue barriers, which sustains immunochemical homeostatic interactions of tissues with internal and external environments.

It has been well determined that one of the essential constituents of tissue barriers is mesenchymal stromal cells (MSCs) [6-9]. Although MSCs are considered to be ubiquitously integrated into conjunctive, vascular, skin, lung, intestinal and other tissues, their major source in the body is the bone marrow, which releases MSCs upon injury and inflammation [6-9]. The data obtained recently from the research conducted on bone marrow MSCs, which show that these cells display antibacterial and immunomodulatory properties, can moderate septic

toxicosis, and improve survival in experimental sepsis [10-14]. Moreover, the effector system which mediates MSCs response to inflammatory stimuli, such as LPS is comprised of a network of toll-like receptors and pattern-recognition receptors [14]; *e.g.,* the molecular machinery that can also promote inflammatory redox-stress [15-18]. In conjunction with these phenomena, there are numerous data gathered from various models indicating that, paradoxically, the inflammagens directly and indirectly can also induce the cellular pro-survival adaptive mechanisms mediated by the redox-response elements and autophagy [18-27]. So far there is only limited information on the adaptive mechanisms enabled in MSCs under inflammatory conditions [14, 28]. In part it could be due to complicity of architecture of mesenchymal network in tissues. Therefore, in the current work we explored primary cultures of mouse bone marrow MSCs challenged with lipopolysaccharide (LPS) inflammagen.

We hypothesized that: (i) a challenge of MSCs with LPS could result in the redox stress; (ii) the adaptive response of MSCs to the redox stress was accompanied by up-regulation of the redox-response factors such as thioredoxin-1 (Trx1), apurinic apyrimidinic endonuclease redox effector factor-1 (Ref1), nuclear factors NFκB, forkhead box O3a (FoxO3a), and NF-E2-related factor 2 (Nrf2), heme oxygenase 1 (HO1), and autophagy; and (iii) activation of autophagy in the LPS-challenged MSCs was to enable remodeling of the damaged cellular constituents including mitochondria. The objective of this communication is to provide experimental evidence of a potential role of MSCs in sustaining redox homeostasis of tissue barriers under the septic oxidative stress.

2 Materials and Methods

Mouse bone marrow mesenchymal stromal cells (MSCs) phenotype and features are well defined in recent reviews [5, 14]. The establishment of MSC cultures used in the presented research was described previously [11] when they were determined to be the bone marrow colony-forming unit fibroblasts [11, 29]. They lack hematopoietic and endothelial lineage markers (CD45, CD34, CD4, and CD117) but are positive for a wide variety of other cell surface molecules (CD44, CD105, and Sca1). The cells expressed collagen type III, matrix metalloproteinases type 3, 9 and 13, and responded to stimulation with the platelet-derived growth factor. These cells were expanded and cultivated in hypoxic conditions (5% O_2, 10% CO_2, 85% N_2) in MESENCULT medium (STEMCELL Technologies Inc.).

MSC cultures were growing till approximately 80% confluency prior to being used in the experiments. LPS (Sigma-Aldrich Co., cat. #L4391) from *E. coli* 0111:B4 were used in concentrations of 0.05-2.5 μg/ml. Challenge of MSCs with LPS was conducted in a "pulse" mode for 1-3 h; and then, incubation medium was replaced with a fresh one. Pyrrolidine dithiocarbamate (PDTC, 10 μM) was used to inhibit NFκB-mediated response to the LPS challenge as reported recently [30].

The challenged cells were either fixed or harvested and, then lysed at different time-points following LPS-challenge (1-24 h). The obtained cell lysates were kept frozen at -80 ^{o}C until further analyses. The LPS-induced gene and protein expressions were determined by qRT-PCR and immunoblotting techniques. Fluorescence imaging techniques were used for (i) assessment of nuclear translocation of p65 subunit of NFκB, i.e., (p65) NFκB, thioredoxin 1 (TRX1), Ref1, and nuclear factor (erythroid-derived 2)-like 2, (Nrf2), (ii) expression and activity of iNOS, (iii) assessment of formation of ROS and RNS with Dihydrorhodamine 123 assay; (iv) assessment

of apoptotic transformations with Annexin V assay; (v) formation of LC3-containing autophagosomes and mitochondrial fusion; and (vi) estimation of proliferative activity with Ki67 marker. LPS-induced mitochondrial remodeling and mitophagy, i.e., autophagy of mitochondria, was demonstrated through transmission electron microscopy (TEM).

For qRT-PCR analyses total cellular RNA was isolated from MSCs using the Qiagen RNeasy miniprep kit, quantified by measuring the absorbance at 260nm on a Nanodrop, and qualified by electrophoresis on a 1.2% agarose gel. cDNA was synthesized using Superscript II (Invitogen) and qRT-PCR was performed using SYBR Green iQ Supermix (Bio-Rad), each according to the manufacturers' instructions. The following primer sequences were used for qRT-PCR: iNOS Forward 5' CAGCTGGGCTGTACAAACCTT 3'; iNOS Reverse 5' CATTGGAAGTGAAGCGTTTCG 3'; IL-1a Forward 5' CGGGTGACAGTATCAGCAAC 3'; IL-1a Reverse 5' GACAAACTTCTGCCTGACGA 3'; IL-1b Forward 5' CCCAACTGGTACATCAGCAC 3'; IL-1b Reverse 5' TCTGCTCATTCACGAAAAGG 3'; IL-6 Forward 5' AGTCGGAGGCTTAATTACACATGTT 3'; Il-6 Reverse 5' AAGTGCATCATCGTTGTTCATACA 3'; IL-8 Forward 5' GCGCCTATCGCCAATGAG 3'; IL-8 Reverse 5' AGGGCAACACCTTCAAGCTCT 3'. The quality of qRT-PCR data were verified by melt curve analysis, efficiency determination, agarose gel electrophoresis, and sequencing. Relative gene expression was calculated by the method of Pfaffl using the formula $2^{-\Delta\Delta Ct}$.

For protein analyses MSCs were lysed and total proteins were extracted in accordance with the protocol described previously [11]. Aliquots of proteins were resolved on SDS-polyacrylamide slab gels (NuPAGE 4-12% Bis-Tris; Invitrogen, Carlsbad, CA). After electrophoresis, proteins were blotted onto a PDVF membrane and the blots were incubated with antibodies (1 µg/ml) raised against MAP LC3, Nrf2, (p65)NFκB, HSP70, Sirt3, p62/SQSTM1, HO1, iNOS, and actin

(Abcam, Santa Cruz Biotechnology Inc., EMD Millipore, and Sigma-Aldrich, Co.) followed by incubation with species-specific IgG peroxidase conjugate.

For expression and spatial localization of proteins in MSCs the cells (5 specimens per group) were fixed in 2% paraformaldehyde, processed for immunestaining and analyzed with fluorescence confocal microscopy [11]. Normal donkey serum and antibody were diluted in phosphate-buffered saline (PBS) containing 0.5% BSA and 0.15% glycine. Any nonspecific binding was blocked by incubating the samples with purified normal donkey serum (Santa Cruz Biotechnology, Inc., Santa Cruz, CA) diluted 1:20. Primary antibodies were raised against MAP LC3, iNOS, Ref1, Trx1, (p65)NFκB, Nrf2, FoxO3a, p53, and Tom 20 (a mitochondrial marker). That was followed by incubation with secondary fluorochrome-conjugated antibody and/or streptavidin-AlexaFluor 610 conjugate (Molecular Probes, Inc., Eugene OR), and with Heochst 33342 (Molecular Probes, Inc., Eugene OR) diluted 1:3000. Secondary antibodies used were AlexaFluor 488 and AlexaFluor 594 conjugated donkey IgG (Molecular Probes Inc., Eugene OR). Negative controls for nonspecific binding included normal goat serum without primary antibody or with secondary antibody alone. Five confocal fluorescence and DIC images of crypts (per specimen) were captured with a Zeiss LSM 710 microscope. The immunofluorescence image analysis was conducted as described previously [12].

Analysis of nitric oxide (NO) formation in LPS-challenged MSC. DAF-FM diacetate (4-amino-5-methylamino-2',7'-difluorofluorescein diacetate, Life Technologies, Inc.) was utilized for detection of NO formation in living cells 24 h after challenge with LPS (500 ng/ml). DAF-FM is essentially nonfluorescent until it reacts with NO to form a fluorescent benzotriazole. The reagent solution (5 μM in PBS) was applied to the cells and a formation of the fluorescent adduct was monitored with a confocal Zeiss LSM 710 microscope using excitation and emission

wavelengths of 485 and 538 nm, respectively. L-N^6 -(1-iminoethyl)lysine (LNIL, Sigma-Aldrich, Co.), a selective inhibitor of iNOS, was used for suppression of NO production in the cells.

Dihydrorhodamine 123 (DhRho 123, Life Technologies, Inc.) was utilized for detection of formation of ROS and RNS (i.e., peroxynitrite) in the cells 24 h after challenge with LPS (500 ng/ml). Dihydrorhodamine 123 is an uncharged and nonfluorescent reactive oxygen species (ROS) indicator that can passively diffuse across membranes where it is oxidized to cationic rhodamine 123 which localizes in the mitochondria and the cytoplasm and exhibits green fluorescence. The reagent solution (10 μM in PBS) was applied to the cells and a formation of the fluorescent product was monitored with a confocal Zeiss LSM 710 microscope L-N^6 -(1-iminoethyl)lysine (LNIL, Sigma-Aldrich, Co), a selective inhibitor of iNOS, was used for suppression of NO release and the consequent RNS-dependent oxidation of DhRho 123 in the cells.

For transmission electron microscopy (TEM) MSCs in culture were fixed in 4% formaldehyde and 4% glutaraldehyde in PBS overnight, post-fixed in 2% osmium tetroxide in PBS, dehydrated in a graduated series of ethanol solutions, and embedded in Spurr's epoxy resin. Blocks were processed as described previously [11]. The sections of embedded specimens were analyzed with a Philips CM100 electron microscope.

Statistical significance was determined using Student's *t*-test for independent samples. Significance was reported at a level of $p<0.05$.

3 RESULTS

In the first set of experiments we assessed alterations in the MSC stress-response-proteins following LPS-challenge. LPS, a major component of the outer membrane of gram-negative bacteria, is considered to be a strong inflammagen. In stromal cells, LPS-induced activation of Toll-like receptor type 4 triggers a danger signal leading to nuclear translocation of NF-**κ**B and subsequent up-regulation of several known inflammatory mediators including iNOS producing NO [14, **26**, 30]. Ultimately, LPS-induced effects can result in redox stress.

As previously published, control MSCs have relatively high amounts of constitutive NF-κB [11]. Confocal immunofluorescence imaging of (p65) NF-κB revealed in controlled MSCs its protein immunoreactivity was predominantly present in the cytoplasm (Fig. 1A). The (p65) NF-κB projections in LPS-challenged cells are shown in Fig. 1B. These data suggest that the challenge of the cells with LPS promoted a prompt (within 1 h) increase in the nuclear fraction of NF-κB (Fig. 1B, indicated with arrows). The nuclear translocation of (p50)(p65) NF-κB is considered to be a part of anti-apoptotic response to stress-induced factors [14, 19]. Therefore, pre-incubation of MSCs with 10 μM PDTC, an inhibititor of the NF-κB pathway, suppressed nuclear translocation of (p65) NF-κB (Fig. 1C) that was accompanied by pro-apoptotic transformations and a loss of cell confluency after application of LPS (Fig. 1D). A summary of quantitative assessment of these LPS-induced effects is presented in a histogram in Fig. 1E. As shown in the last figure (Fig. 1E, d) an increase in nuclear translocation of (p65) NF-κB was observed in almost all MSCs treated with 500 ng/ml LPS (3h-pulse) 24 h post-treatment. The observed LPS-induced trans-activation of NF-κB in MSCs was accompanied by a drastic expression of pro-inflammatory mediators including IL-1α, IL-1β, IL-6, and iNOS that occurred in a dose-dependent manner (Table 1, qRT-PCR analysis).

A maximum expression of iNOS was observed at a dose of 500 ng/ml LPS (Table 1); therefore, our further experiments on LPS-induced MSC toxicity were conducted using this dose. It should be noted that while MSCs displayed resistance to substantially higher doses of LPS (up to 5000 ng/ml) they experienced inhibition of proliferative activity under those conditions (data not shown). Moreover, there is evidence (Dr. Elliott TB, unpublished data) that the LPS dose 500 ng/ml blood can induce in mice a severe septic syndrome with a predicted mortality rate 80-90%.

LPS pulse-challenge for 3 h resulted in a prolong changes in redox-status of MSCs. Thus, 24 h after the LPS challenge we observed increase in (p65) NFκB translocation in ≈90% of the treated MSCs (Fig. 1E), that was accompanied by a dramatic accumulation of iNOS protein in the cells (Fig. 2). The immunoblotting data presented in Fig. 2 were confirmed by immunofluorescence imaging of iNOS protein in the cells (Fig. 3). Accumulation of iNOS resulted in excessive production of NO in the cells determined by increase in fluorescence intensity of the fluorescent adduct of DAF-FM with NO in the LPS-treated cells (Figs. 4 A,B). This effect was suppressed in the presence of LNIL, a specific iNOS inhibitor (Fig. 4 C). An increase in the formation of ROS and RNS associated with the LPS stimulation was monitored with DhRho 123, another molecular probe, which is subjected to oxidation in the presence of ROS and peroxynitrite and thus, is converted to fluorescent Rho 123. The results of DhRho imaging in the cells are presented in Fig. 5. As shown, in the control cells a moderate Rho 123 fluorescence appeared only in mitochondria, a major generator of ROS under normal condition (Fig. 5A). Dramatic changes in Rho 123 fluorescence were observed in the LPS-challenged cells: the increase in fluorescence was observed not only in the confocal projections of mitochondria; the entire cytoplasm emitted green fluorescence (Fig. 5B). Interestingly, elongation of mitochondria due to activation of mitochondrial fusion was observed under these

conditions (Fig. 5B). This increase in Rho 123 fluorescence was suppressed in the presence of LNIL, a specific iNOS inhibitor (Fig. 5C). Overall, the presented data suggested that the LPS-challenged cells experienced the redox-stress due to increase in iNOS-dependent production of NO. Therefore, we expected up-regulation of the redox-response elements mediating cell adaptation to long-lasting stress conditions.

It is well accepted that numerous vitagenes are evolutionarily adapted by cells to manage oxidative stress; they include but are not limited to redox-sensitive transcriptional factors, antioxidants, heat shock proteins, and regulators of autophagy and mitochondrial functions [22, 24, 25, 27, 31-37]. As follows from our results presented in Fig. 2, a 3 h-pulse challenge of MSCs with LPS resulted in a substantial increase in NFκB in the cell protein fraction. NFκB is known as a redox-sensitive transcription factor that contains a critical cysteine residue (Cys-62) in the p50 subunit that is involved in DNA binding [24,36]. NFκB is normally present in the cytoplasm in a complex with the inhibitory subunit IkB but under oxidative conditions, IkB is phosphorylated by I-kB kinase (IKK), ubiquitinated and subsequently degraded. Excessive oxidative stress can lead to the oxidation of Cys-62 which does not affect its translocation to the nucleus but rather interferes with DNA binding and decreases gene trans-activation [24,38]. Therefore, in the presence of oxidative stress nuclear translocation of activated (p50)(p65)NFκB has to be synchronized with increase in nuclear fraction of reductants TRX1 and Ref1 [24,38]. Overall, while the NFκB system has been recognized to be primarily activated by inflammagenes (such as LPS) via Toll-like and other receptors, it was the first mammalian transcription factor determined to be redox regulated and suggested to be directly activated by ROS and RNS [24,36,38].

Confocal projections of cellular NFκB shown in Fig. 6 A-F indicate a relatively low level of nuclear fraction of NFκB in control cells. This balance dramatically changed after challenge

with LPS (Fig 6. H-N). That was associated with increases in nuclear fractions of TRX1, i.e., a reducing factor essential for activation of oxidized nuclear (p50)NFκB (Figs. 7); note the localization of nuclear TRX1 appeared in close proximity with nuclear (p65)NFκB (Fig. 6).

One of the most crucial cellular defense mechanisms against oxidative stress and nitrosative stress is mediated by the transcription factor Nrf2 [23, 24, 33, 38, 39]. Under the basal condition, Nrf2 is compartmentalized in the cytoplasm and Nrf2-dependent transcription is repressed by a negative regulator Keap1. In the presence of ROS an RNS Nrf2 is released from a complex with Keap1, translocated to the nucleus where it activates antioxidant responsive element (ARE)-dependent gene expression to maintain cellular redox homeostasis [23, 24, 40]. In this respect, mechanisms of "sensing" the redox stress by Nrf2 seems similar to that one demonstrated for NFκB. Therefore, it was not surprising that the patterns of up-regulation of Nrf2 and NFκB in the LPS-challenged MSCs were similar (Figs. 2,6,7); with exception that in contrast to NFκB we did not observe a significant increase in nuclear fraction of Nrf2 at 1 h-pulse LPS-challenge of the cells (data not shown) as we did with NFκB.

At this stage it was reasonable to assume that deep metabolic changes essential for long-term survival of the cells under redox stress conditions may proceed via a cascade of events which are driven by synchronous activation (or suppression) of different signaling mechanisms. As example, we tested LPS-induced nuclear translocation of two other transcriptional factors, i.e., FoxO3a and p53. FoxO3a, a member of a family of mammalian forkhead transcription factors of the class O, has been was recently proposed as mediator of diverse physiologic processes, including regulation of resistance to redox stress and increase in longevity [31, 32]. In opposite to FoxO3a, p53 transcriptional factor is the well-discussed master regulator of apoptotic cell death, which can be activated in stromal cells by redox genotoxic stress [41]. The effects of LPS-challenge on nuclear translocation of FoxO3a and p53 are

shown in Fig. 8. Indeed, as expected a massive increase in nuclear fractions of FoxO3a occurred in the LPS-treated cells (Fig. 8; control panels A1, A2 *vs*. LPS-treatment panels B1, B2) that corroborated with effects observed for Nrf2 and NFκB (Figs. 6 and 7). Meanwhile, there were no any significant changes in nuclear immunofluorescence of p53 protein (Fig. 8; control panels C1, C2 *vs*. LPS panels D1, D2).

The analyzed above transcriptional factors, i.e., Nrf2, NFκB, and FoxO3a, are implicated in regulation of a variety of adaptogens, antioxidants, and mediators of autophagy and mitochondrial remodeling including HSP70, HO1, p62, Sirt3, and LC3 [23, 24, 33, 35, 42]. Moreover, a growing body of evidence suggests involvement of chaperone heat-shock proteins and adaptor proteins in autophagy events [42, 43]. The results of immunoblot analyses of these proteins in the LPS-treated MSCs are shown in Fig. 9 (Panel A). LPS-induced expression of HSP70 and Sirt3 was insignificant (Fig. 9A) and was apparently due to high levels of the constitutively present proteins. Meanwhile, we observed a substantial increase in HO1 protein (Fig. 9B) that was in concord with the LPS-induced response of Nrf2 (Figs. 7 and 9A), a transactivator of HO1 [35].

Remarkable responses occurred in the ubiquitin-associated target adaptor p62/SQSTM1 and LC3 type I and type II proteins (Fig. 9A), which are mediators of macroautophagy (ATPhG) [11, 22, 37, 43]. A key step in the autophagosome biogenesis is the conversion of light-chain protein 3 type I (LC3-I, also known as ubiqitin-like protein, Atg8) to type II (LC3-II). The conversion occurs via the cleavage of the LC3-I carboxyl terminus by a redox-sensitive Atg4 cysteine protease. The subsequent binding of the modified LC3-I to phosphatidylethanolamine, i.e., process of lipidation of LC3-1, on the isolation membrane, as it forms, is mediated by E-1- and E-2-like enzymes Atg7 and Atg3 [11, 22, 37]. Thus, conversion of LC3-I to LC3-II and formation of LC3-positive vesicles are considered to be a marker of activation of ATPhG [11, 22,

37]. As shown in Fig. 9A, a challenge of MSC with LPS resulted in increases in both LC3-I and LC3-II expression as determined by immunoblotting; and indicated up-regulation of the LC3-I to LC3-II transition. At this stage our further investigation was focused on immunofluorescence confocal imaging and TEM analysis of ATPhG -mediated remodeling in the LPS-challenged cells.

In the second set of experiments we analyzed autophagy/autolysosomal response and mitochondrial remodeling in MSCs subjected to LPS-challenge. The ATPhG pathway is considered to be an evolutionarily developed pro-survival mechanism, which removes and processes damaged and misfolded proteins, and compromised organelles in response to redox stress [21, 25, 27, 37, 44]. Activation of ATPhG is associated with formation of autophagic/autolysosomal vacuoles in the cytoplasm which mediate proteolytic processes [11, 22, 25, 27].

The images presented in Fig. 10 indicate that up-regulation of LC3-I/LC3-II proteins in the LPS-challenged cells was associated with massive formation of the LC3-positive vesicles featuring autophagosomes and autolysosomes.

The further assessment of autophagy events with TEM revealed in the LPS-challenged cells the presence of characteristic multiple vacuoles, which were formed by double-layer membranes and sequestered constituents of different densities (Fig. 10). Some of these vacuoles can be identified as secretory autolysosomes by the presence of multilamellar structures (most likely fibers of collagen) released extracellularly, while others contained fractured organelles including compromised mitochondria (Fig. 11).

Recent observations suggest that autophagosomes do not form randomly in the cytoplasm, but rather sequester mitochondria selectively [45, 46]. Selection of compromised mitochondria for mitophagy requires activation of the PINK1/PARKIN pathway and implication of

adaptor proteins, e.g., p62/SQSTM1, and ubiquitin-like modifiers, which target mitochondria and ultimately mediate fusion of the processed mitochondria with autophagosome [45, 46].

The images presented in Figs. 10 E and 11 B-D indicate that mitochondria can be fused with autophagosomes of similar sizes while further degradation occurred in large-size autolysosomes.

The observed mitophagy was accompanied by extensive mitochondrial fusion resulting in the remodeling and expansion of the mitochondrial network (Figs. 11 and 12). The events of mitochondrial fusion and formation of elongated mitochondria (over 10 μm length) were captured with TEM and confocal immunofluorescence microscopy and are presented in Figs. 11 E, F and 12D. All the above data suggest that a short-term challenge with LPS triggered in MSCs a battery of complex adaptive responses leading to an increase in resistance to redox stress and damage to cellular constituents, and also to the remodeling of the entire mitochondrial network.

4 DISCUSSION

The redox stress occurs in the pathogeneses of a variety of injury types, including radiation combined injury and the associated sepsis; and there are multiple original papers and reviews addressed recently to this phenomenon [4, 14, 47-49]. The associated secondary oxidative injury to sensitive cellular constituents and ER stress can affect homeostasis of tissue barriers and thus, exacerbate the process of healing. With this respect, development of new regiments for treatment of complicated injuries can be made more efficient with better understanding of the basic cellular mechanisms implicated in redox adaptive responses in

tissue barriers. This particular area of the molecular redox pathophysiology is poorly developed despite the general concept of cellular stress responses is broadly discussed in the literature [35, 38, 50]. Our communication is the first report demonstrating a potential role of MSCs in sustaining redox resistance of barrier functions under septic conditions.

According to the current paradigm, general stress responses involve conserved signaling modules that, in turn, are interconnected to the cellular adaptive mechanisms [21, 33, 50]. It has been shown recently that bacterial infections trigger specific sensitive mechanisms mediating inflammation, redox stress, adaptation, and remodeling [2, 3, 17, 20, 21, 22]. Redox stress *per se* stimulates signaling cascades mediated by transcription factors and pathways that are believed to play a central role in cell survival. These include, but are not limited to, a battery of thiol-containing redox-response elements, redox-sensitive transcription factors such as nuclear factor-kappa B (NFκB), Nrf2, FoxO3a, and stress-response adaptors such as the chaperone heat-shock protein 70 (HSP70) and NAD^+-dependent deacetylase sirtuin-3 (Sirt3), and activators of the autolysosomal degradation and mitochondrial remodeling. Overall, these effector systems are crucial in maintaining homeostasis, which is altered due to oxidative damage to cell constituents [35-46]. It should be noted that, while the role of the redox-induced NFκB and Nrf2 responses in cell survival is well documented, transcriptional factor FoxO3a, the autophagy/autolysosomal pathway, and mitochondrial remodeling are relatively newly-determined players implicated into adaptive mechanisms [21, 30, 31, 36, 37, 42-46].

Recently we demonstrated *in vitro* that MSCs could employ ATPhG in phagocytosis of *Escherichia coli* [11]. However, a mechanism which allowed the cells to avoid the adverse effects of the products of bacterial biodegradations, such as LPS, yet remained unclear. The data presented in this report indicate that *in vitro* challenge of MSCs with LPS inflammagen triggered a cascade of responses that we believe to orchestrate adaptive remodeling of the cell

and to increase resistance to a “self-inflicted” LPS-induced oxidative stress. A pattern of these adaptive responses include induction of redox-response elements such as NFkB, TRX1, Ref1, Nrf2, FoxO3a, and activation of ATPhG and mitochondrial remodeling. It should be noted that despite the presence of mitophagy and mitochondrial remodeling in the LPS-challenged MSCs there was no significant alterations in levels of Sirt3 protein, which was a major player in mitochondrial response to the redox-stress [35, 37, 46]. We assumed that it was likely due to a high constitutive expression of this protein in MSCs. Meanwhile, unlike Sirt3, there occurred a significant expression of HO1, an antioxidant protein, which utilized mitochondrial heme, which *per se* is a catalyst of the Fenton type of reactions as well as is essential for the *de novo* formation of active form of iNOS [35, 51]. Overall, our observations support a general concept of the presence of a network of a variety of signaling pathways that enable to mediate cellular adaptation to the oxidative stress [33, 35, 37, 40, 43, 50].

5 Acknowledgements

The authors thank Mr. Areya Tabatabai and Ms. Joan Smith for their technical supports.

Grants

This work was supported by AFRRI Intramural RAB3AL (to JGK), NIAID R21/33AI080553 (to JGK), and NIAID Y1-AI-5045-04 (to JGK). There are no ethical and financial conflicts in the presented work.

Disclaimer

The views expressed in this paper do not necessarily represent the Armed Forces Radiobiology Research Institute, the Uniformed Services University of the Health Sciences, NIH, or the US Department of Defense.

6 References

[1] Angus DC, Linde-Zwirble WT, Lidicer J, Clermont G, Carcillo J, Pinsky MR. Epidemiology of severe sepsis in the United States: analysis of incidence, outcome, and associated costs of care. Crit Care Med 2001;29(7):1303-10.

[2] Russell JA. Management of Sepsis. N Engl J Med 2006; 355(16):1699-713.

[3] Kiang JG, Jiao W, Cary L, Mog SR, Elliott TB, Pellmar TC, Ledney GD. Wound trauma increases radiation-induced mortality by increasing iNOS, cytokine concentrations, and bacterial infections. Radiate Res 2010;173:319-332.

[4] Kiang JG, Garrison BR, Gorbunov NV. Radiation combined injury: DNA damage, apoptosis, and autophagy. Adapt Med 2010;2:1-10.

[5] Perl M, Chung CS, Swan R, Ayala A. Role of Programmed Cell Death in the Immunopathogenesis of Sepsis. Drug Discov Today Dis Mech 2007;4(4):223-230.

[6] Krebsbach PH, Kuznetsov SA, Bianco P, Robey PG. Bone marrow stromal cells: characterization and clinical application. Crit Rev Oral Biol Med. 1999;10(2):165-81.

[7] Winkler IG, Barbier V, Wadley R, Zannettino AC, Williams S, Lévesque JP. Positioning of bone marrow hematopoietic and stromal cells relative to blood flow in vivo: serially reconstituting hematopoietic stem cells reside in distinct nonperfused niches. Blood. 2010;116(3):375-85.

[8] Powell DW, Pinchuk IV, Saada JI, Chen X, Mifflin RC. Mesenchymal Cells of the Intestinal Lamina Propria. Annual Review of Physiology. 2011;3:213-37.

[9] Jackson WM, Alexander PG, Bulken-Hoover JD, Vogler JA, Ji Y, McKay P, Nesti LJ, Tuan RS. Mesenchymal progenitor cells derived from traumatized muscle enhance neurite growth. J Tissue Eng Regen Med. 2012; doi:10.1002/term.539. [Epub ahead of print].

[10] Krasnodembskaya A, Song Y, Fang X, Gupta N, Serikov V, Lee JW, Matthay MA. Antibacterial effect of human mesenchymal stem cells is mediated in part from secretion of the antimicrobial peptide LL-37. Stem Cells. 2010;28(12):2229-38.

[11] Gorbunov NV, Garrison BR, Zhai M, McDaniel DP, Ledney GD, Elliott TB, Kiang JG. Autophagy-Mediated Defense Response of Mouse Mesenchymal Stromal Cells (MSCs) to Challenge with *Escherichia coli*. In: Protein Interaction/Book 1; ISBN 979-953-307-577-7. Eds.: Cai J. InTech Open Access Publisher. Page 23–44.

[12] Le Blanc K, Ringdén O. Immunomodulation by mesenchymal stem cells and clinical experience. J Intern Med. 2007;262(5):509-25.

[13] Lee JW, Fang X, Gupta N, Serikov V, Matthway MA. Allogeneic human mesenchymal stem cells for treatment of E. coli endotoxin-induced acute lung injury in the ex vivo perfused human lung. Proc Natl Acad Sci USA. 2009;106(38):16357-62.

[14] Nemeth K, Mayer B, Mezey E. Modulation of bone marrow stromal cell functions in infectious diseases by toll-like receptor ligands. J Mol Med. 2010;88(1):5-10.

[15] Kobayashi KS, Chamaillard M, Ogura Y, Henegariu O, Inohara N, Nuñez G, Flavell RA. Nod2-dependent regulation of innate and adaptive immunity in the intestinal tract. Science. 2005;307(5710):731-4.

[16] Imai Y, Kuba K, Neely GG, Yaghubian-Malhami R, Perkmann T, van Loo G, Ermolaeva M, Veldhuizen R, Leung YH, Wang H, Liu H, Sun Y, Pasparakis M, Kopf M, Mech C, Bavari S, Peiris JS, Slutsky AS, Akira S, Hultqvist M, Holmdahl R, Nicholls J, Jiang C, Binder CJ, Penninger JM. Identification of oxidative stress and Toll-like receptor 4 signaling as a key pathway of acute lung injury. Cell. 2008;133(2):235-49.

[17] Gill R, Tsung A, Billiar T. Linking oxidative stress to inflammation: Toll-like receptors. Free Radic Biol Med. 2010;48(9):1121-32.

[18] Lecat A, Piette J, Legrand-Poels S. The protein Nod2: an innate receptor more complex than previously assumed. Biochem Pharmacol. 2010;80(12):2021-31.

[19] Sebban H, Courtois G. NF-kappaB and inflammation in genetic disease. Biochem Pharmacol. 2006;72(9):1153-60.

[20] Thimmulappa RK, Lee H, Rangasamy T, Reddy SP, Yamamoto M, Kensler TW, Biswal S. Nrf2 is a critical regulator of the innate immune response and survival during experimental sepsis. J Clin Invest. 2006;116(4):984-95.

[21] Murrow L, Debnath J. Autophagy as a Stress-Response and Quality-Control Mechanism: Implications for Cell Injury and Human Disease. Annu Rev Pathol. 2012 Oct 15. [Epub ahead of print]

[22] Delgado M, Singh S, De Haro S, Master S, Ponpuak M, Dinkins C, Ornatowski W, Vergne I, Deretic V. Autophagy and pattern recognition receptors in innate immunity. Immunol Rev. 2009;227(1):189-202.

[23] Brigelius-Flohé R, Flohé L. Basic principles and emerging concepts in the redox control of transcription factors. Antioxid Redox Signal. 2011;15(8):2335-81.

[24] Nguyen T, Nioi P, Pickett CB. The Nrf2-antioxidant response element signaling pathway and its activation by oxidative stress. J Biol Chem. 2009;284(20):13291-5.

[25] Yuan H, Perry CN, Huang C, Iwai-Kanai E, Carreira RS, Glembotski CC, Gottlieb RA. LPS-induced autophagy is mediated by oxidative signaling in cardiomyocytes and is associated with cytoprotection. Am J Physiol Heart Circ Physiol. 2009; 296(2):H470-9.

[26] Crisostomo PR, Wang Y, Markel TA, Wang M, Lahm T, Meldrum DR. Human mesenchymal stem cells stimulated by TNF-alpha, LPS, or hypoxia produce growth factors by an NF kappa B- but not JNK-dependent mechanism. Am J Physiol Cell Physiol. 2008;294(3):C675-82.

[27] Jin Y, Tanaka A, Choi AM, Ryter SW. Autophagic proteins: new facets of the oxygen paradox. Autophagy. 2012;8(3):426-8.

[28] Iyer SS, Torres-Gonzalez E, Neujahr DC, Kwon M, Brigham KL, Jones DP, Mora AL, Rojas M. Effect of bone marrow-derived mesenchymal stem cells on endotoxin-induced oxidation of plasma cysteine and glutathione in mice. Stem Cells Int. 2010; 2010:868076.

[29] Owen M, Friedenstein AJ. Stromal stem cells: marrow-derived osteogenic precursors. Ciba Found Symp 1988;136:42-60.

[30] Zhang JJ, Xu ZM, Zhang CM, Dai HY, Ji XQ, Wang XF, Li C. Pyrrolidine dithiocarbamate inhibits nuclear factor-κB pathway activation, and regulates adhesion, migration, invasion and apoptosis of endometriotic stromal cells. Mol Hum Reprod. 2011;17(3):175-81.

[31 Burhans WC, Heintz NH. The cell cycle is a redox cycle: linking phase-specific targets to cell fate. Free Radic Biol Med. 2009; 47:1282-93.

[32] Sengupta A, Molkentin JD, Paik JH, DePinho RA, Yutzey KE. FoxO transcription factors promote cardiomyocyte survival upon induction of oxidative stress. J Biol Chem. 2011; 286(9):7468-78.

[33] Maher J, Yamamoto M. The rise of antioxidant signaling--the evolution and hormetic actions of Nrf2. Toxicol Appl Pharmacol. 2010;244(1):4-15.

[34] Go YM, Duong DM, Peng J, Jones DP. Protein Cysteines Map to Functional Networks According to Steady-state Level of Oxidation. J Proteomics Bioinform. 2011;4(10):196-209.

[35] Calabrese V, Cornelius C, Dinkova-Kostova AT, Iavicoli I, Di Paola R, Koverech A, Cuzzocrea S, Rizzarelli E, Calabrese EJ. Cellular stress responses, hormetic phytochemicals and vitagenes in aging and longevity. Biochim Biophys Acta. 2012; 1822(5):753-83.

[36] Martin LJ. Biology of mitochondria in neurodegenerative diseases. Prog Mol Biol Transl Sci. 2012;107:355-415.

[37] Lee J, Giordano S, Zhang J. Autophagy, mitochondria and oxidative stress: cross-talk and redox signalling. Biochem J. 2012;441(2):523-40.

[38] Jones DP. Radical-free biology of oxidative stress. Am J Physiol Cell Physiol. 2008 295(4):C849-68.

[39] Um HC, Jang JH, Kim DH, Lee C, Surh YJ. Nitric oxide activates Nrf2 through S-nitrosylation of Keap1 in PC12 cells. Nitric Oxide. 2011;25(2):161-8.

[40] Maruyama A, Nishikawa K, Kawatani Y, Mimura J, Hosoya T, Harada N, Yamamato M, Itoh K. The novel Nrf2-interacting factor KAP1 regulates susceptibility to oxidative stress by promoting the Nrf2-mediated cytoprotective response. Biochem J. 2011;436(2):387-97.

[41] Gorbunov NV, Morris JE, Greenberger JS, Thrall BD. Establishment of a novel clonal murine bone marrow stromal cell line for assessment of p53 responses to genotoxic stress. Toxicology. 2002; 179(3):257-66.

[42] Rinaldi Tosi ME, Bocanegra V, Manucha W, Gil Lorenzo A, Vallés PG. The Nrf2-Keap1 cellular defense pathway and heat shock protein 70 (Hsp70) response. Role in protection against oxidative stress in early neonatal unilateral ureteral obstruction (UUO). Cell Stress Chaperones. 2011;16(1):57-68.

[43] Fujita K, Maeda D, Xiao Q, Srinivasula SM. Nrf2-mediated induction of p62 controls Toll-like receptor-4-driven aggresome-like induced structure formation and autophagic degradation. Proc Natl Acad Sci U S A. 2011;108(4):1427-32.

[44] Yang Z, Klionsky DJ. Mammalian autophagy: core molecular machinery and signaling regulation. Curr Opin Cell Biol. 2010; 22(2):124-31.

[45] Reggiori F, Komatsu M, Finley K, Simonsen A. Selective types of autophagy. Int J Cell Biol 2012;2012:156272.

[46] Kubli DA, Gustafsson AB. Mitochondria and mitophagy: the yin and yang of cell death control. Circ Res. 2012; 111(9):1208-21.

[47] Kagan VE, Day BW, Elsayed NM, Gorbunov NV. Dynamics of haemoglobin. Nature 1996; 383(6595):30-2.

[48] Keel M, Trentz O. Pathophysiology of polytrauma. Injury. 2005 36(6):691-709.

[49] Kiang JG, Fukumoto R, Gorbunov NV. (2012) Lipid peroxidation after ionizing irradiation leads to apoptosis and autophagy. In: Lipid Peroxidation; Ed.: Angel Catala. Rijeka: InTech Open Access Publisher; DOI: 10.5772/2929; pp. 261-278. ISBN 978-953-51-0716-3. http://www.intechopen.com/books/lipid-peroxidation.

[50] Kültz D. Molecular and evolutionary basis of the cellular stress response. Annu Rev Physiol. 2005;67:225-57.

[51] Piantadosi CA. Carbon monoxide, reactive oxygen signaling, and oxidative stress. Free Radic Biol Med. 2008; 45:562–9.

Figure Legends

Table 1. qRT-PCR assessment of gene transcription in MSCs challenged with LPS.

Conditions: MSCs were incubated with 50 ng/ml – 2500 ng/ml LPS for 3 h, and then were lysed for mRNA extraction and qRT-PCR analysis. The presented data are statistically significant at the confidence levels $p < 0.005$, (n=3).

Fig 1. Confocal immunofluorescence assessment of nuclear translocation of (p65) NFκB in MSCs following stimulation with LPS.

Panels A-C are Overlay of projections of nuclei (blue channel) and (p65) NFκB (red channel) in MSCs.

Panel A – Control cells.

Panel B – MSCs challenged with 500 ng/ml LPS for 1 h. Activation of (p65)NFκB nuclear translocation was defined by increase in immunofluorescence of (p65)NFκB in the nuclear regions. Nuclear regions of MSCs were determined by counterstaining of nuclear DNA with Hoechst 33342 (blue channel). Nuclear localization of (p65) NFκB appears in purple (indicated with arrows).

Panel C – Same as Panel "B" except MSCs were pre-incubated with 10 μM PDTC (pyrrolidine dithiocarbamate), an inhibitor of NFκB.

Panel D – The treatments were the same as in Panel "C" but the presented image is overlay of projections of Annexin V (green channel), a marker of pro-apoptotic transformations, and a respective DIC image of MSCs. Apoptotic events are indicated with arrows.

The confocal images were taken with pinhole setup to obtain 0.5 μm Z-sections. Conditions: MSCs were incubated with 500 ng/ml LPS in the medium either 1 h or 3 h (see Methods).

Panel E – Histogram depicting increase in frequency (per 100 cells) of occurrence (p65)NFκB nuclear translocation in MSCs treated with LPS. Spatial appearance of (p65)NFκB in MSCs was determined with immunofluorescence confocal microscopy as indicated in Methods. Confocal projections of nuclear fractions of (p65)NFκB are shown in panels A-C.

Fig 2. Immunoblot analysis of expression of NFκB and iNOS proteins in MSCs subjected to LPS challenge.

Panel A. Immunoblotting bands of NFκB and iNOS.

Panel B. Densitometry histograms of iNOS bands in MSCs subjected to challenge with LPS. The presented bars indicate the relative density of iNOS protein (normalized to density of actin bands). The statistical significance was determined by Student's *t*-test (n=3).

Conditions: MSCs were incubated with 500 ng/ml LPS for 3 h. The cells were harvested at 24 h following challenge with LPS.

Fig 3. Confocal immunofluorescence imaging of iNOS protein in MSCs challenged with LPS.

Panel A1 - Projections of nuclei (blue channel) in control MSCs: Panel A2 - Projections of iNOS (red channel); Panel A3 – overlay of projections presented in panels A1 and A2 and a respective DIC image.

Panel B1 - Projections of nuclei (blue channel) in LPS-challenged MSCs: Panel B2 - Projections of iNOS (red channel); Panel B3 – Overlay of projections presented in panels B1 and B2 and a respective DIC image. A massive accumulation of iNOS occurred in the LPS-challenged MSCs. Counterstaining of nuclei was with Hoechst 33342 (blue channel). The confocal images were taken with pinhole setup to obtain 0.5 μm Z-sections. Conditions were the same as indicated in Fig. 2.

Fig 4. Confocal immunofluorescence imaging of the DAF-FM –detectable nitric oxide in MSCs challenged with LPS.

Panel A1 - Projection of adduct of DAF-FM with NO (DAF-FM-NO) (green channel) in control MSCs; Panel A2 – Overlay of projection of DAF-FM-NO shown in A1 and a respective DIC image; Panel A3 – Histogram of relative fluorescence of DAF-FM-NO shown in A1.

Panel B1 - Projection of adduct of DAF-FM-NO (green channel) in LPS-challenged MSCs; Panel B2 – Overlay of projection of DAF-FM-NO shown in B1 and a respective DIC image. A dramatic increase in DAF-FM-NO fluorescence occurred in the LPS-challenged MSCs.

Panel C1 – C3 – Same as B1 – B3 except LPS-challenged MSCs were treated with LNIL, an iNOS inhibitor. Suppression of DAF-FM-NO fluorescence occurred in the LPS-challenged MSCs.

Fig 5. Confocal immunofluorescence imaging of the DhRho 123–detectable ROS/RNS products in MSCs challenged with LPS.

Panel A1 - Projection of oxidized form of DhRho 123 (Rho 123) (green channel) in control MSCs; Panel A2 – Overlay of projection of Rho 123 shown in A1 and a respective DIC image.

Panel B1 - Projection of Rho 123 (green channel) in LPS-challenged MSCs; Panel B2 – Overlay of projection of Rho 123 shown in B1 and a respective DIC image. A dramatic increase in Rho 123 fluorescence occurred in the LPS-challenged MSCs.

Panel C1 - Projection of Rho 123 (green channel) in LPS-challenged MSCs and treated with LNIL, an iNOS inhibitor; Panel C2 – Overlay of projection of Rho 123 shown in C1 and a respective DIC image. Suppression of Rho 123 fluorescence occurred in the LPS-challenged MSCs.

Bright green fluorescence of the ROS-activated Rho 123 shown in mitochondria is shown with red arrows. Diffused green fluorescence of the ROS/RNS-activated Rho 123 in the cytoplasm is shown with white arrows in panel B.

The confocal images were taken with pinhole setup to obtain 0.5 μm Z-sections. The experimental conditions were the same as indicated in Fig. 2.

Fig 6. Confocal immunofluorescence imaging of nuclear translocation of NFκB and thioredoxin 1 (TRX1) in MSCs challenged with LPS.

Panels A - C. Projections of (p65)NFκB (red channel) and TRX1 (green channel) in control MSCs.

Panel D. Overlay of projections of (p65)NFκB, TRX1, and nuclei presented in panels “A-C”.

Panel E. ROI selected in panel “D”.

Panel F. Histogram of immunofluorescence of (p65)NFκB in nuclei shown in panel E.

Panel G. Histogram of immunofluorescence of TRX1 in nuclei shown in panel E.

Panels H - J. Projections of (p65)NFκB (red channel) and TRX1 (green channel) in LPS-challenged MSCs.

Panel K. Overlay of projections of (p65)NFκB, TRX1, and nuclei presented in panels "H-J".

Panel L. ROI selected in panel "K".

Panels M and N. Histograms of immunofluorescence of (p65)NFκB and TRX1 in nuclei shown in panel L.

Counterstaining of nuclei was with Hoechst 33342 (blue channel). The confocal images were taken with pinhole setup to obtain 0.5 μm Z-sections. The experimental conditions were the same as indicated in Fig. 2.

Fig 7. Assessment of nuclear translocation of Nrf2 redox-response element in MSCs challenged with LPS.

Counterstaining of nuclear DNA was with Hoechst 33342 (blue channel). Nrf2 staining is in green. Nrf2 localized in nuclei appears in turquoise/green color due to interference of "green" and "blue" (indicated with arrows). Experimental conditions were the same as indicated in Fig. 2.

Fig 8. Assessment of nuclear translocation of FoxO3a and p53 redox-response element in MSCs challenged with LPS.

Counterstaining of nuclear DNA was with Hoechst 33342 (blue channel). FoxO3a staining is in red (control panels A1, A2 *vs*. LPS-treatment panels B1, B2). Panels A2 and B2 are overlay of confocal projections of FoxO3a protein (red channel) and nuclear DNA (blue channel). FoxO3a nuclear translocation is indicated with arrows in Panels B1 and B2; where nuclear fraction of FoxO3a appears in pink color due to interference of "red" and "blue" (Panel B).

Panels C1, C2, D1, D2 – Confocal projections of p53 protein (red channel) in MSCs (control panels C1, C2 *vs*. LPS panels D1, D2). Counterstainings were done with Hoechst 33342 (for nuclear DNA, blue channel) and anti-TOM20 IgG (for mitochondria, green cannel). Panels C2 and D2 are overlay of confocal projections of p53 protein (red channel), TOM20 protein (green

channel) and nuclear DNA (blue channel). Note, there was no detectable increase in the p53-immunofluorescence in nuclear areas of LPS-challenged MSCs. The confocal images were taken with pinhole setup to obtain 0.5 μm Z-sections.

Experimental conditions were the same as indicated in Fig. 2.

Fig 9. Western immunoblot analysis of redox-response and autophagy-mediated proteins in MSCs challenged with LPS.

Panel A. Representative immunoblotting bands of HSP70, Nrf2, p62/SQSTM1, Sirt3, and LC3 proteins. The protein extracts were obtained from MSC cultures 24 h after challenge with LPS.

Panels B and C. Representative immunoblotting bands of Hemeoxygenase 1 (HO1) protein (B) and respective densitometry histograms of HO1 bands (C) in MSCs stimulated with LPS. The presented bars indicate the relative density of HO1 protein (normalized to density of actin bands). The statistical significance was determined by Student's *t*-test (n=3). Conditions: MSCs were incubated with 500 ng/ml LPS for 3 h. The cells were harvested at 24 h following challenge with LPS.

Fig 10. Assessment of autophagosome formation in MSCs challenged with LPS.

Panels A - D Confocal immunofluorescence imaging

Panel A – (Green channel). LC3 projection in control MSCs.

Panel B – Overlay of projections of LC3 (green channel), iNOS (red channel), and nuclei (blue channel) in control MSCs.

Panel C – (Green channel). LC3 projection in MSCs challenged with LPS.

Panel D – Overlay of projections of LC3 (green channel), iNOS (red channel), and nuclei (blue channel) in MSCs challenged with LPS. Spatial localization of LC3 is indicated with white arrows.

Conditions: MSCs were incubated with 500 ng/ml LPS for 3 h. The cells were analyzed 24 h after challenge with LPS. Counterstaining of nuclei was with Hoechst 33342 (blue channel). The confocal images were taken with pinhole setup to obtain 0.5 μm Z-sections.

Panel E is TEM image of MSCs challenged with LPS. Autophagosome (ATG) membranes are indicated with yellow arrows; fragments of mitochondrion in ATG is indicated with white arrow; fusion of lysosomes with ATG is indicated with pink arrow.

Fig. 11. Transmission electron (TEM) analysis of mitochondrial remodeling in MSCs challenged with LPS.

Panel A: Image of a control MSC. Mitochondria are indicated with yellow arrows.

Panels B-F – Images of MSCs challenged with LPS.

Panel B – Damaged mitochondria subjected remodeling and mitophagy are shown with red arrows. Double-layer membrane of an auotolysosome is indicated with white arrow. Mt, mitochondrium.

Panels C and D – Fusion of damaged mitochondria (Mt) with autophagosomes (ATG) is indicated with red arrows. ATG membranes are indicated with white arrows.

Panel D – Formation of secretory autolysosomes containing multilamellar structures (indicated with red arrows) in an irradiated MSC.

Panel E – Fusion of mitochondria (Mt) is indicated with yellow arrow.

Panel F – Formation of elongated mitochondria is indicated with white arrow. Mitophagy is indicated with red arrow.

Conditions: MSCs were incubated with 500 ng/ml LPS for 3 h. The cells were analyzed 24 h after challenge with LPS.

Fig. 12. Confocal immunofluorescence imaging of mitochondrial remodeling in MSCs challenged with LPS.

Mitochondrial networks were visualized using projections of TOM20 (red channel), a mitochondrial marker.

Panels A and B – Control MSCs: mitochondrial network is presented by small-size dots.

Panels C and D – MSCs challenged with LPS: formation of long-length mitochondrial network occurred due to mitochondrial fusion.

Conditions: MSCs were incubated with 500 ng/ml LPS for 3 h. The cells were analyzed 24 h after challenge with LPS. Counterstaining of nuclei was with Hoechst 33342 (blue channel). The confocal images were taken with pinhole setup to obtain 0.5 μm Z-sections.

Table 1					
LPS	IL1A	IL1ß	IL6	IL8	iNOS
ng/ml	Expression, A.U.	Expression, A.U.	Expression, A.U.	Expression, A.U.	Expression, A.U.
0	1±3.25	1±1.82	1±1.54	1±1.41	1±3.14
50	194±2.77*	317±1.63*	99±1.48*	26±1.8*	882±2.46*
100	265±2.33*	465±1.78*	155±1.4*	46±1.36*	1128±2.3*
500	315±2.35*	755±1.68*	47±2.67*	18±1.98*	1596±2.46*
1000	247±2.38*	498±1.78*	98±1.6*	11±1.61*	1489±2.37*
2500	338±2.35*	729±1.57*	224±2.32*	20±3.3*3	1438±2.25*

*p<0.005, n=3

Table 1

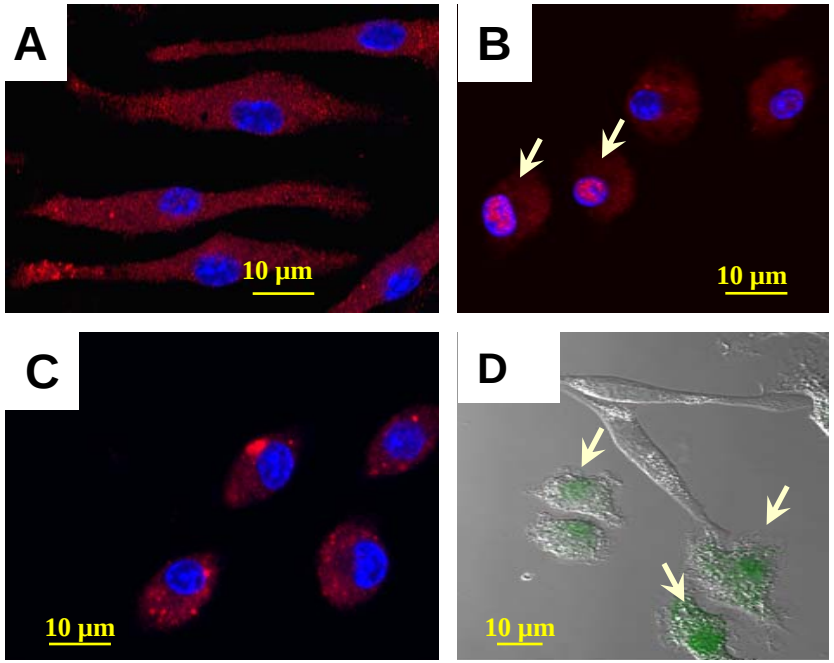

Figs 1A-D

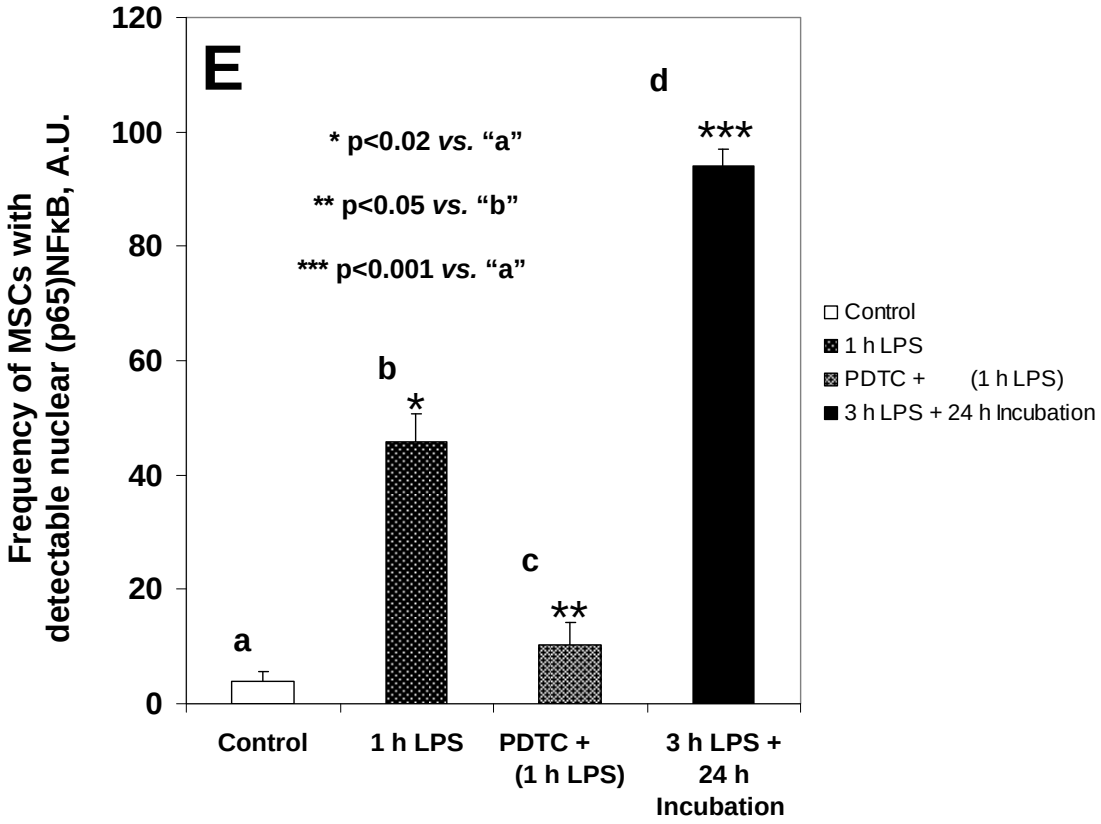
E
Frequency of MSCs with detectable nuclear (p65)NFκB, A.U.
120
100
80
60
40
20
0
* p<0.02 vs. "a"
** p<0.05 vs. "b"
*** p<0.001 vs. "a"
a
b
*
c
**
d
***
Control
1 h LPS
PDTC + (1 h LPS)
3 h LPS + 24 h Incubation
Control
1 h LPS
PDTC + (1 h LPS)
3 h LPS + 24 h Incubation

Fig 1E

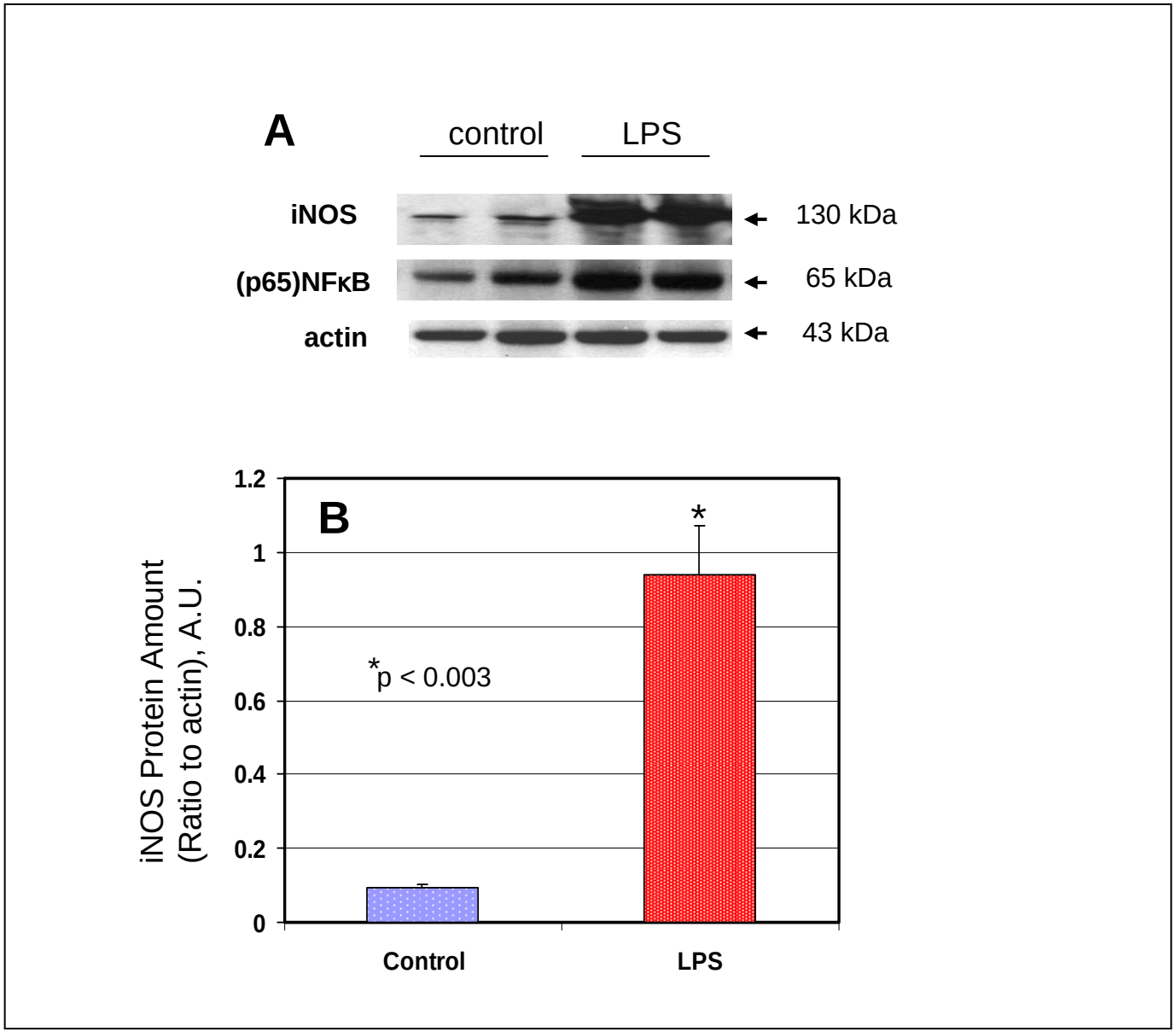
A
control
LPS
iNOS
(p65)NFκB
actin
130 kDa
65 kDa
43 kDa
B
iNOS Protein Amount
(Ratio to actin), A.U.
1.2
1
0.8
0.6
0.4
0.2
0
*
*p < 0.003
Control
LPS

Figs 2 A-B

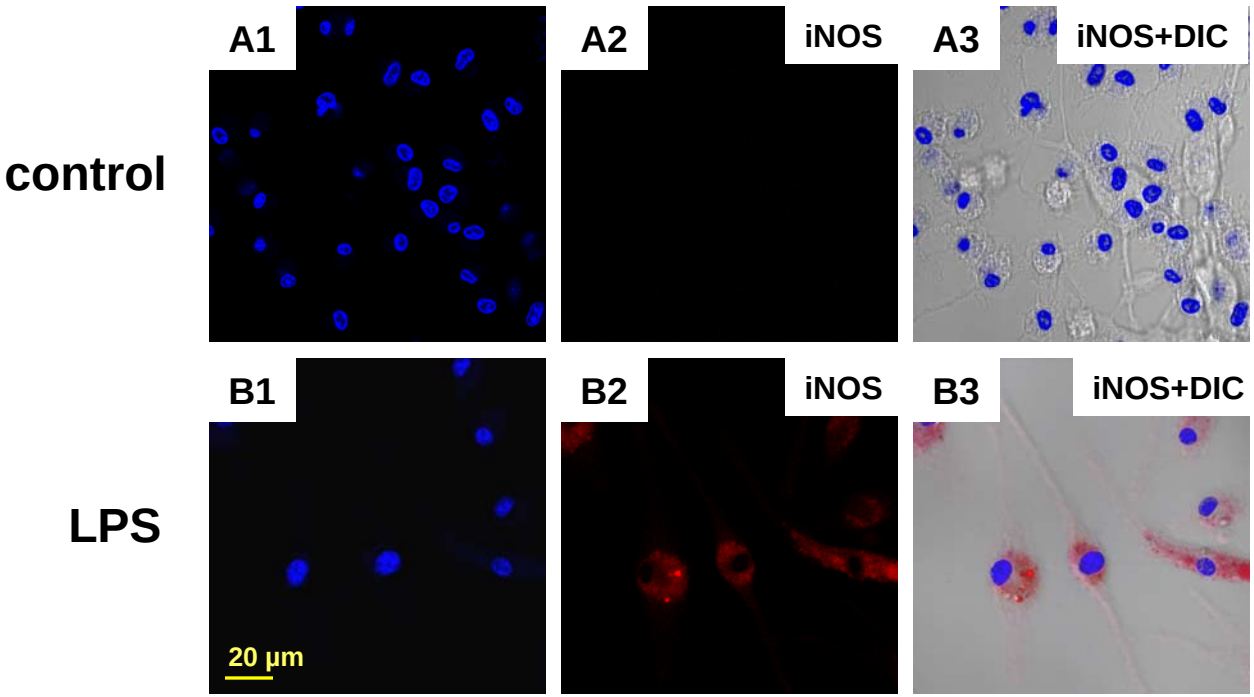

Fig 3

Fluorescence imaging of the LPS-induced NO production in MSC with DAF-FM fluorescent probe

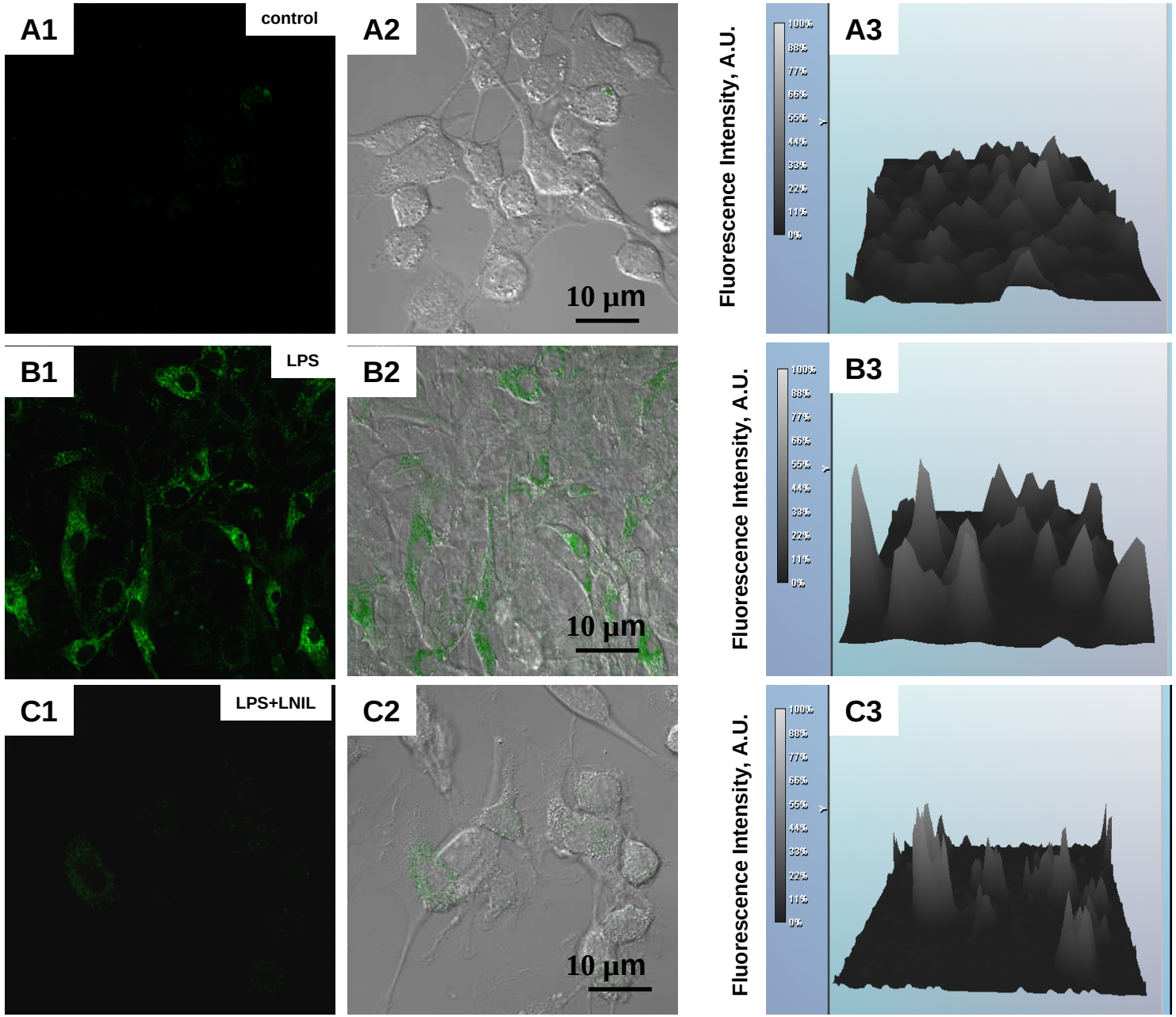

Fig 4

The formation of an adduct of DAF-FM with NO was detected by appearance of green fluorescence in MSC.

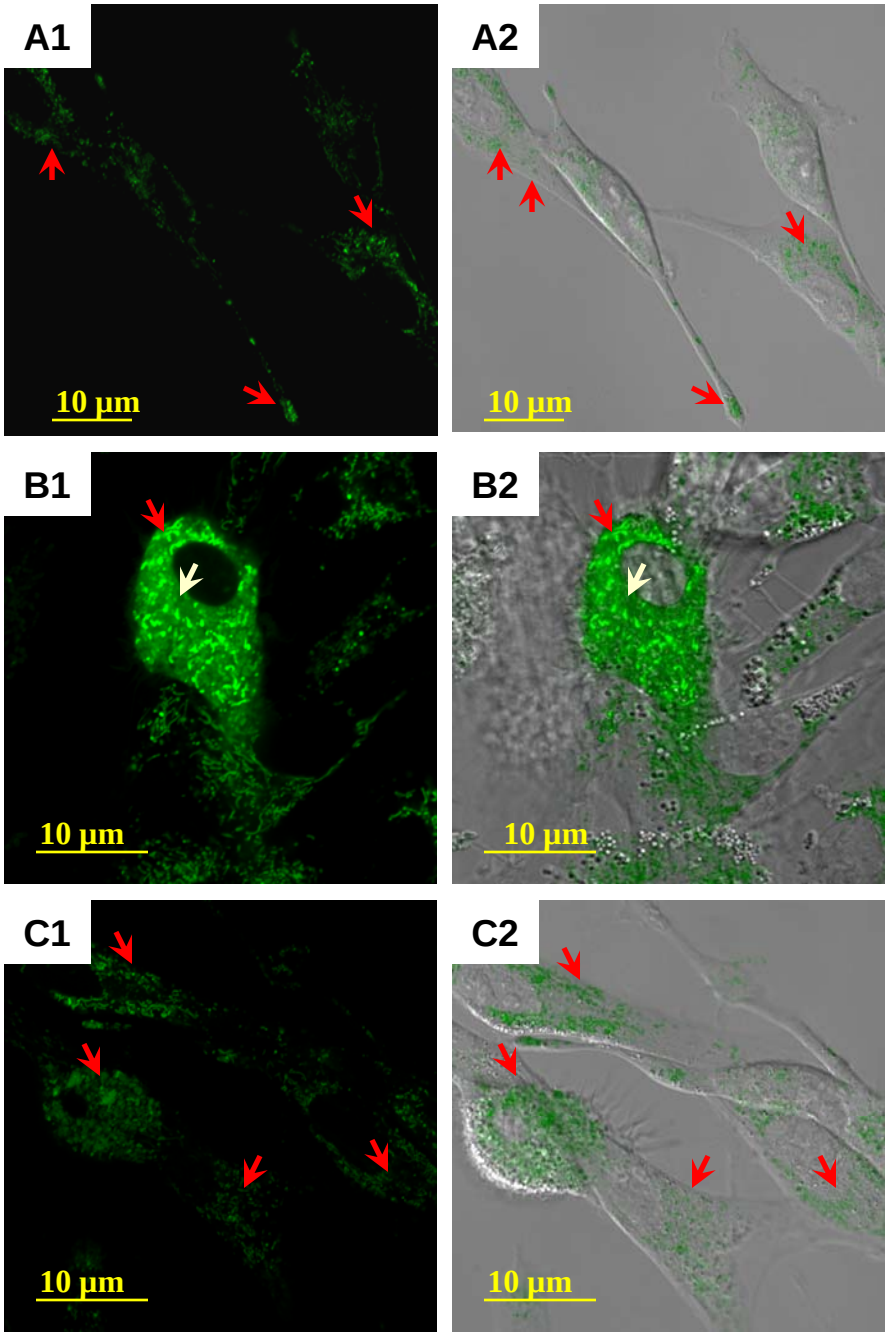

Fig 5

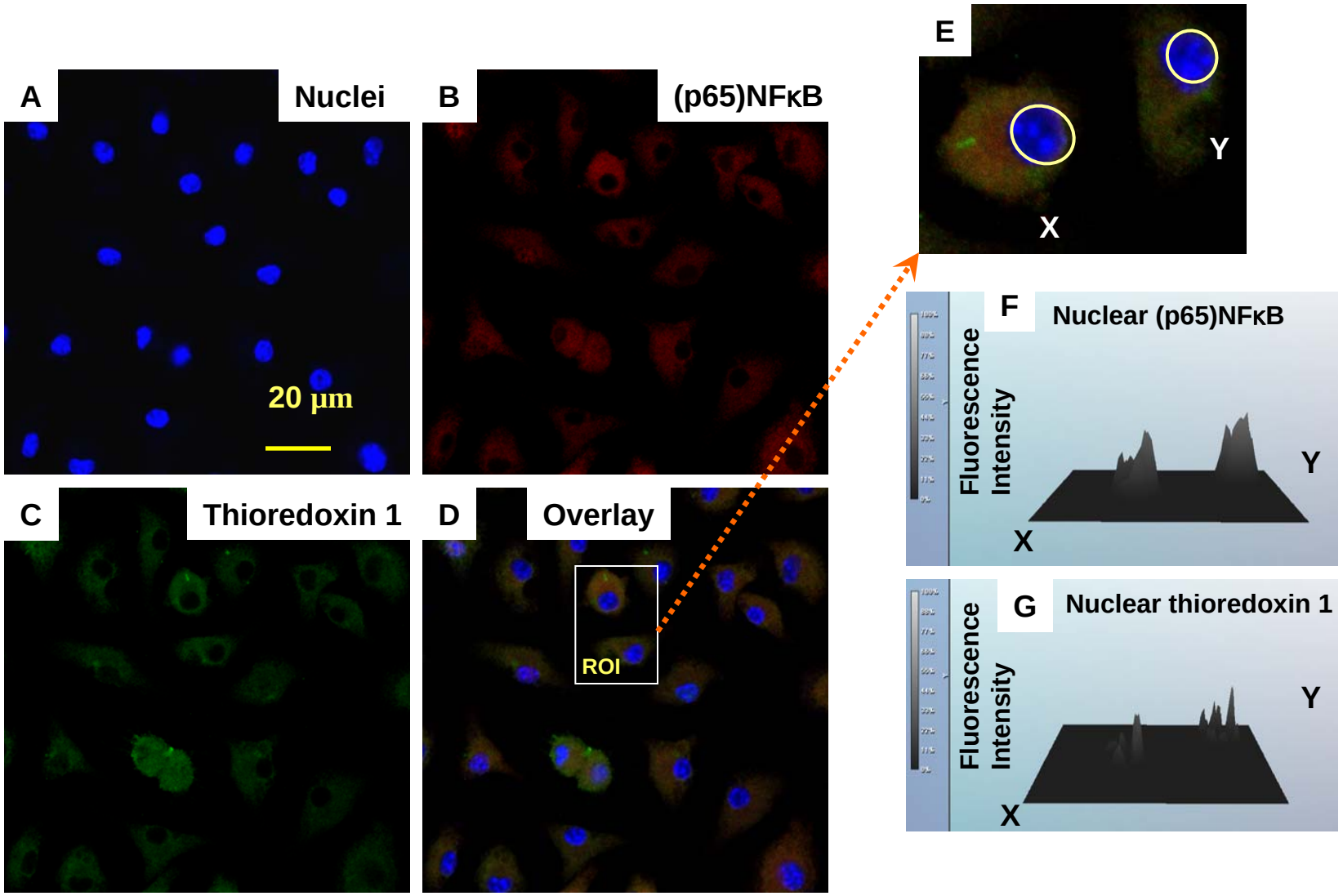
A
Nuclei
B
(p65)NFκB
20 µm
C
Thioredoxin 1
D
Overlay
ROI
E
Y
X
F
Nuclear (p65)NFκB
Fluorescence Intensity
Y
X
G
Nuclear thioredoxin 1
Fluorescence Intensity
Y
X

Figs 6 A-F

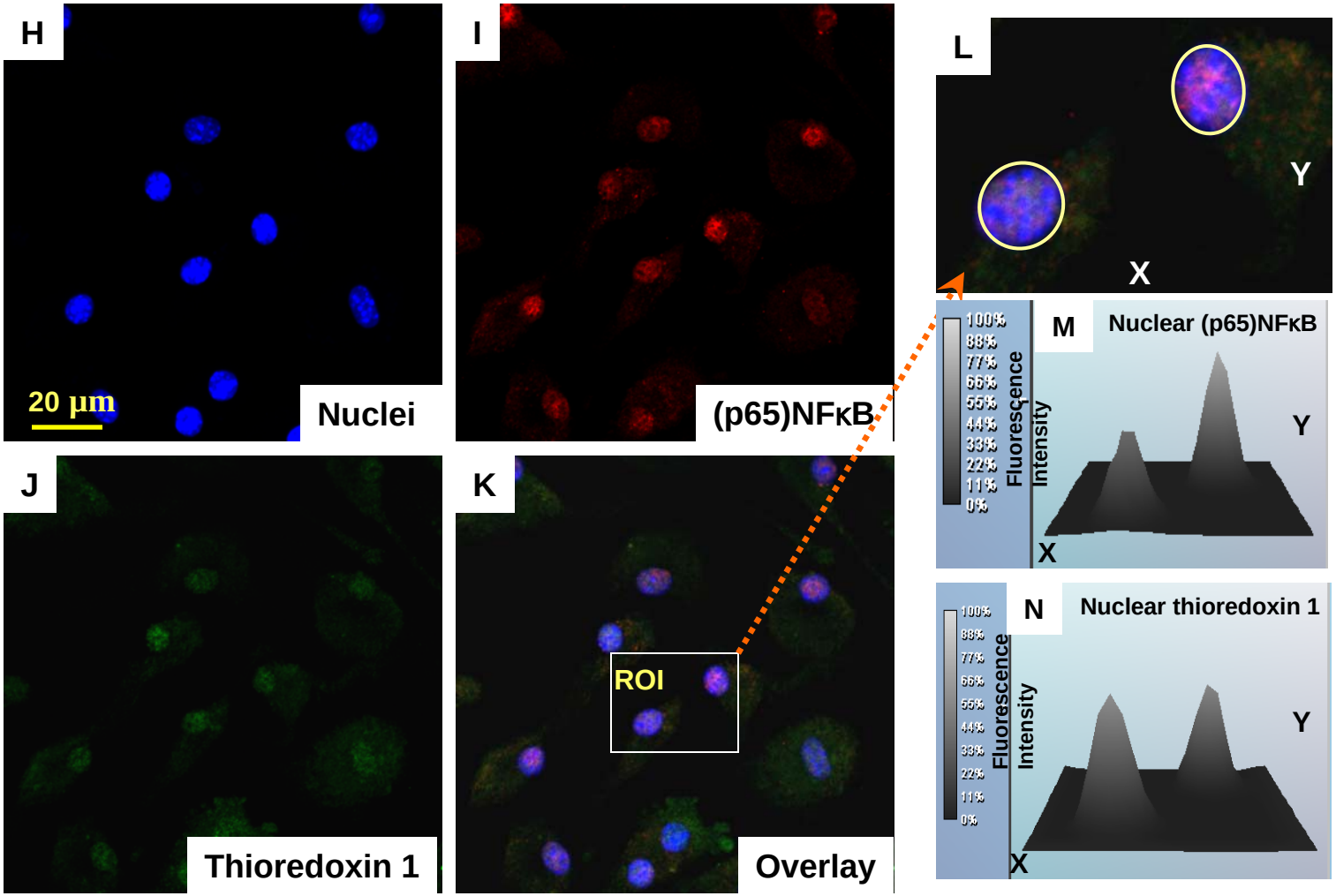
H
20 µm
Nuclei
I
(p65)NFκB
L
Y
X
J
Thioredoxin 1
K
ROI
Overlay
M
Nuclear (p65)NFκB
100%
88%
77%
66%
55%
44%
33%
22%
11%
0%
Fluorescence Intensity
Y
X
N
Nuclear thioredoxin 1
100%
88%
77%
66%
55%
44%
33%
22%
11%
0%
Fluorescence Intensity
Y
X

Figs 6 G-M

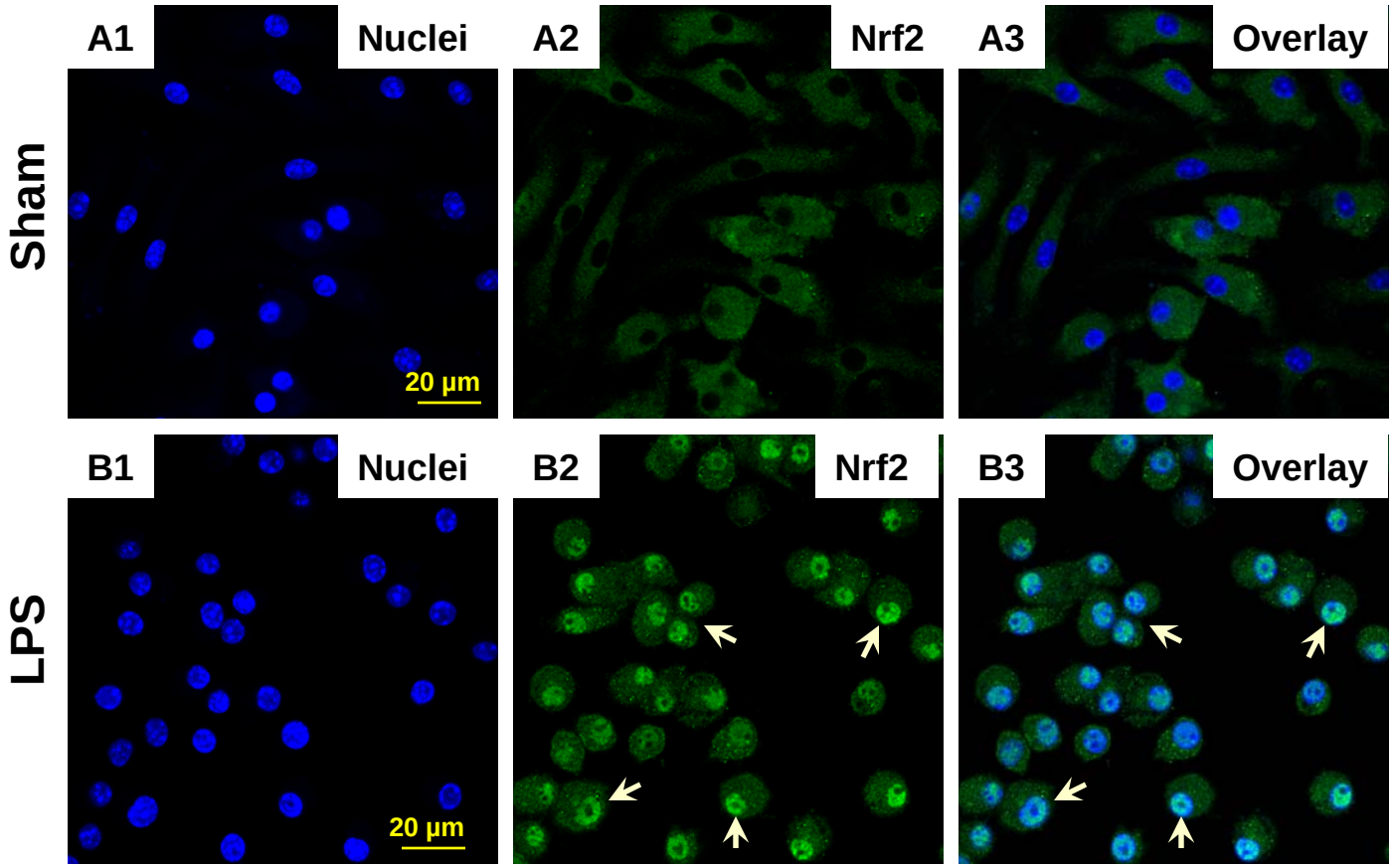
A1
Nuclei
A2
Nrf2
A3
Overlay
Sham
20 µm
B1
Nuclei
B2
Nrf2
B3
Overlay
LPS
20 µm

Fig 7

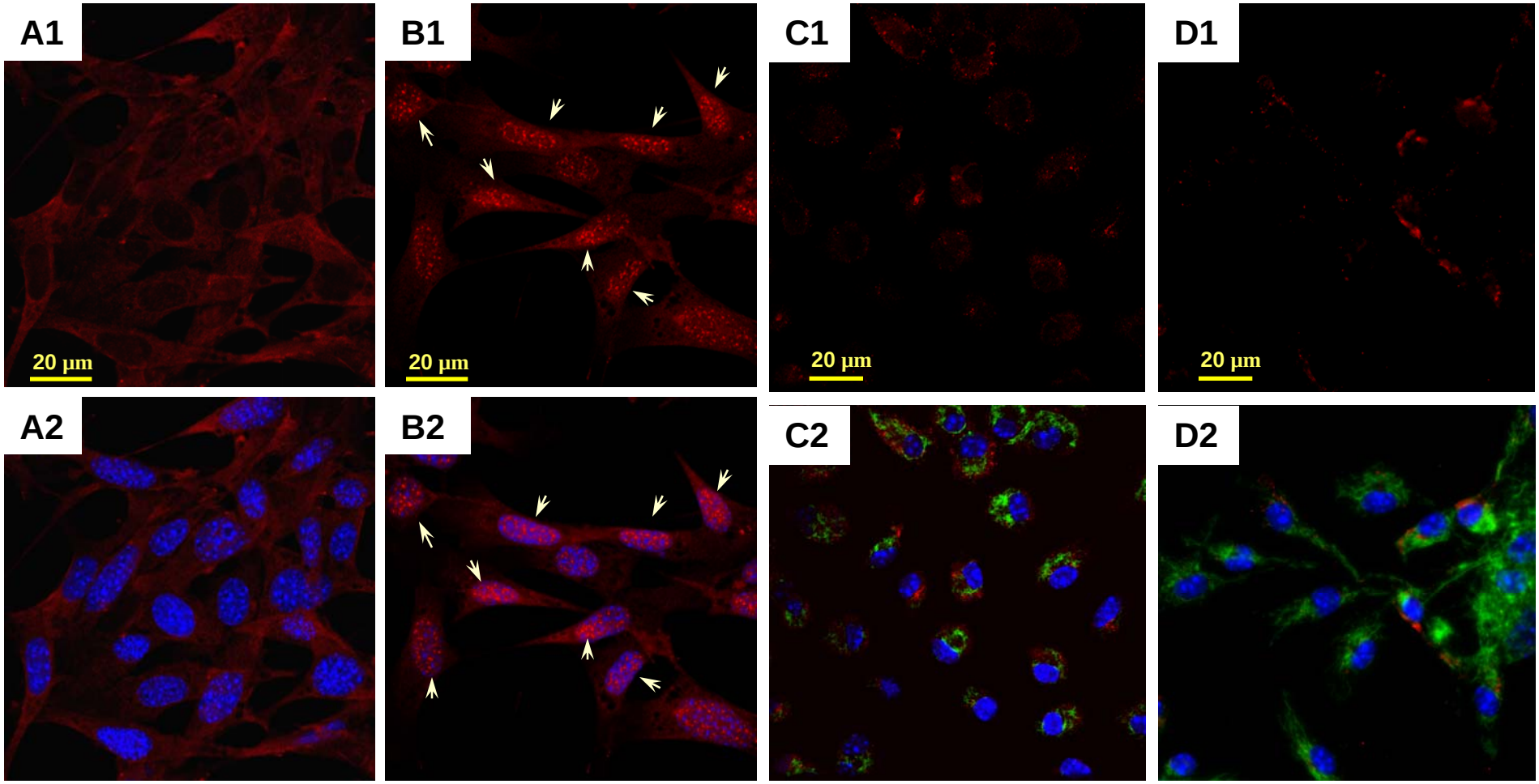

Fig 8

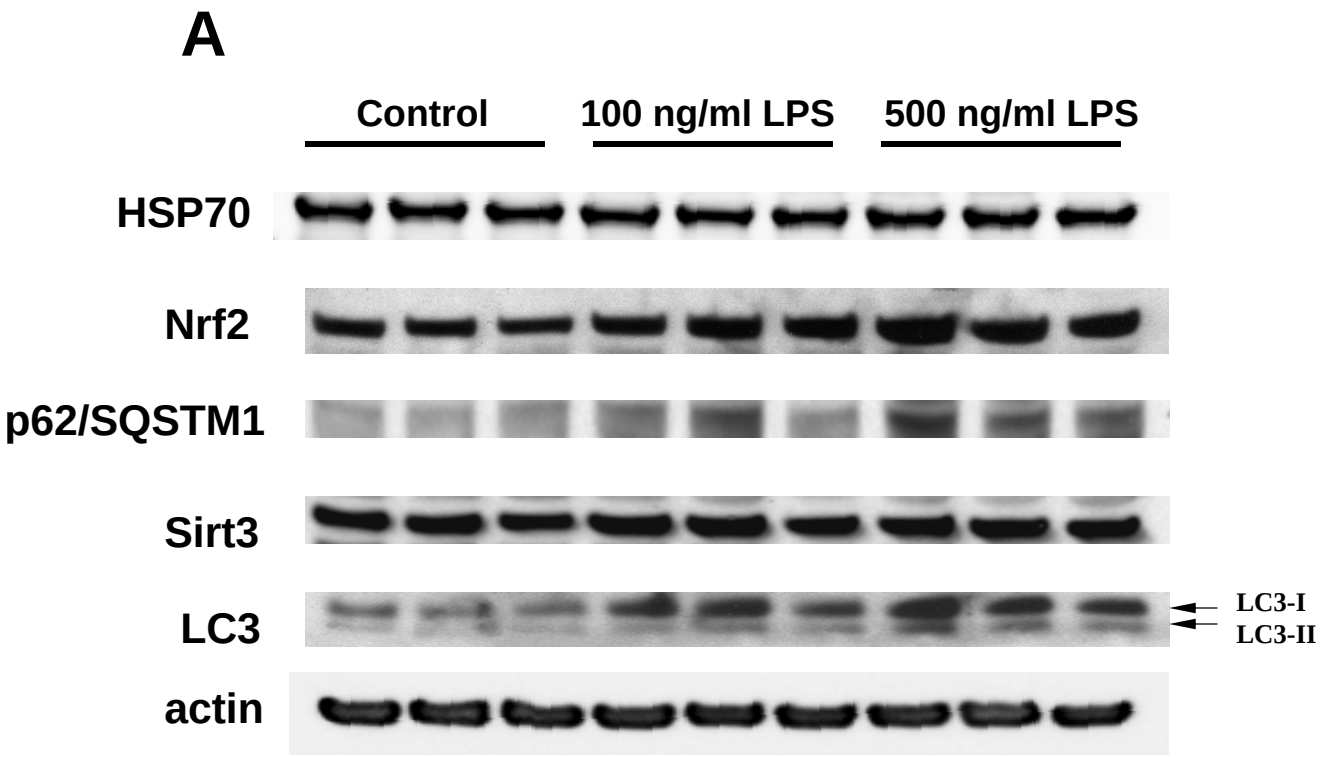
A
Control
100 ng/ml LPS
500 ng/ml LPS
HSP70
Nrf2
p62/SQSTM1
Sirt3
LC3
actin
LC3-I
LC3-II

Fig 9 A

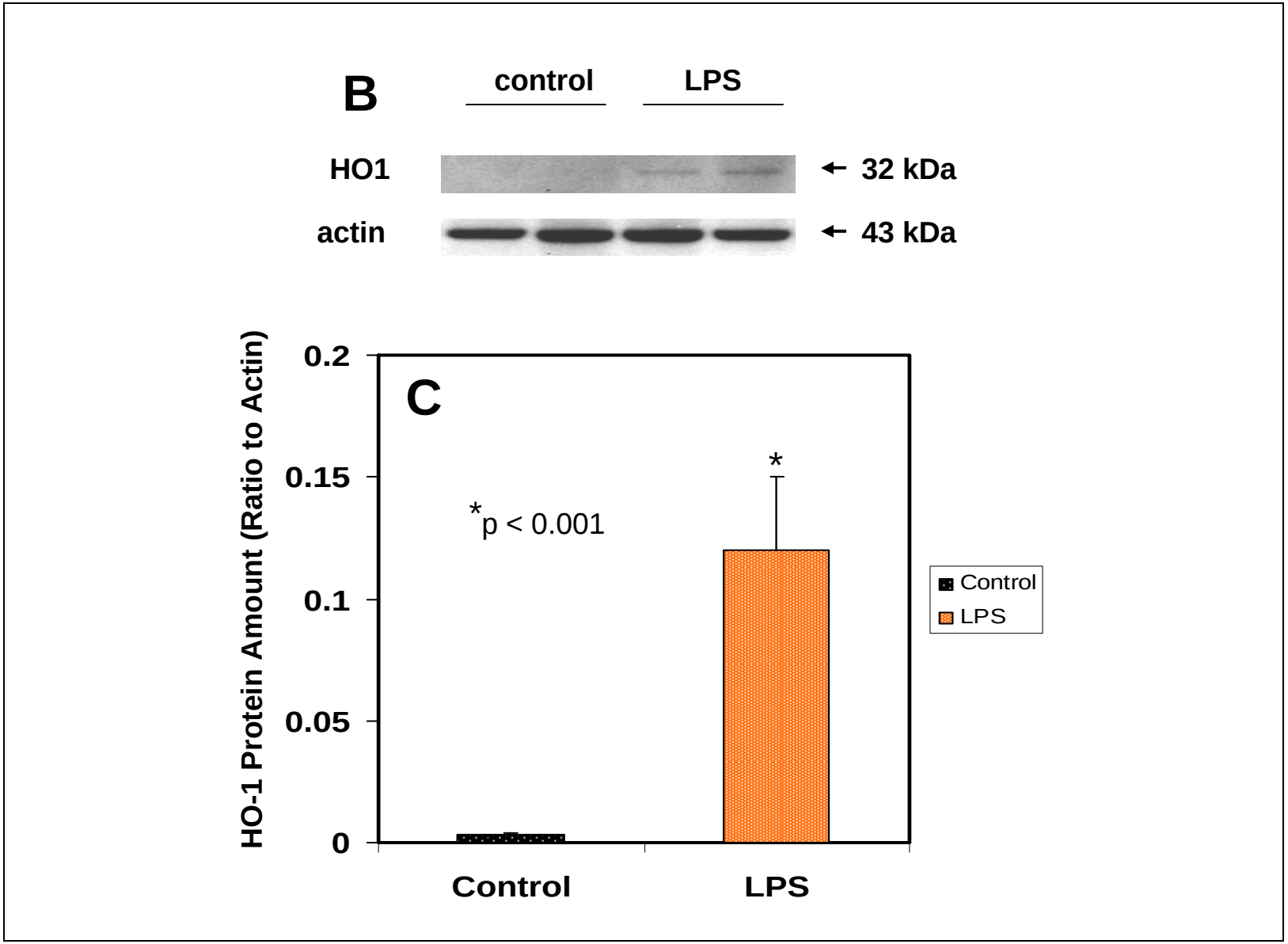
B
control
LPS
HO1
32 kDa
actin
43 kDa
C
HO-1 Protein Amount (Ratio to Actin)
0.2
0.15
0.1
0.05
0
*p < 0.001
*
Control
LPS
Control
LPS

Fig 9 B

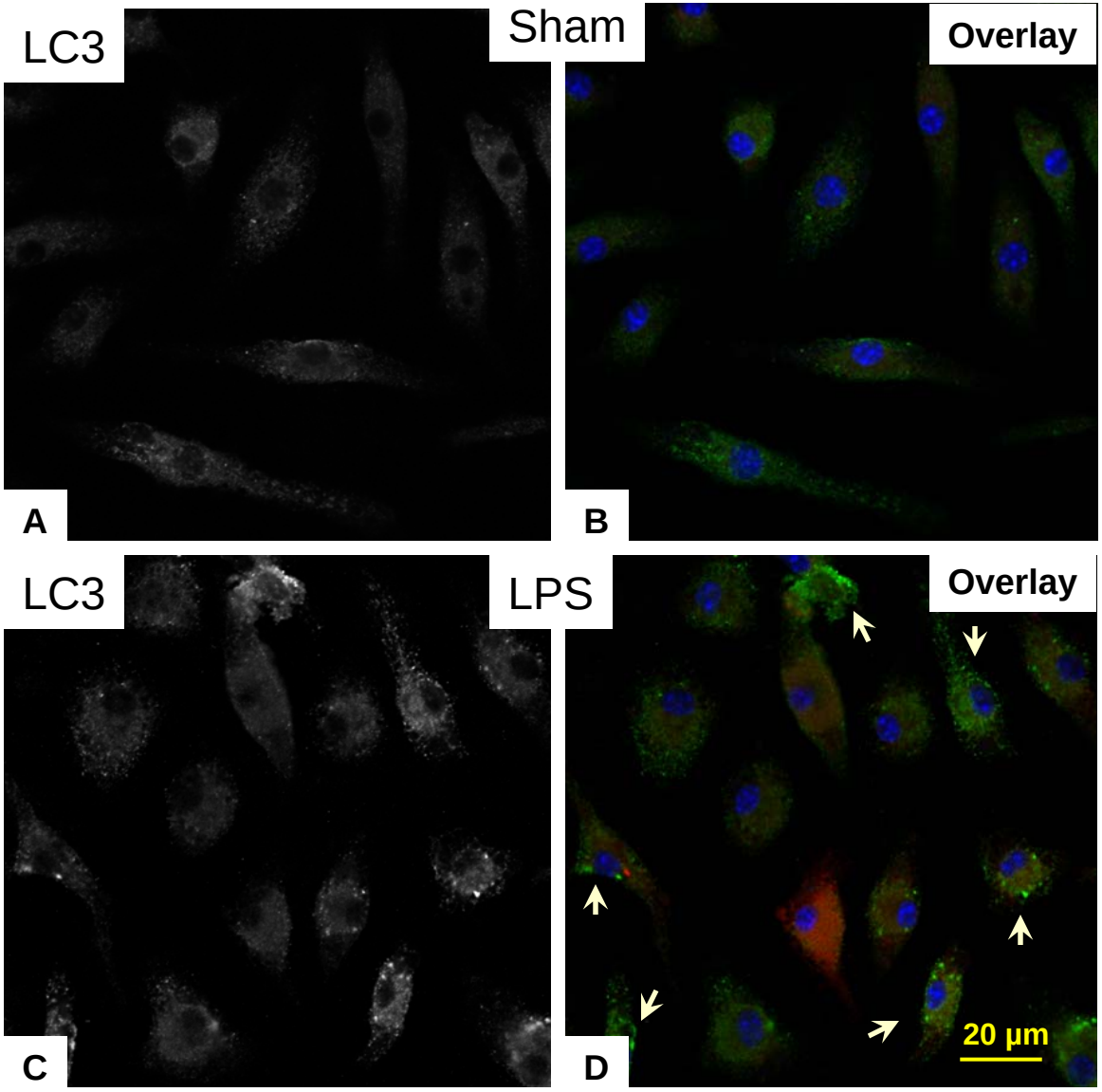
LC3
Sham
Overlay
A
B
LC3
LPS
Overlay
C
D
20 μm
E
ATG
ATG
ATG
500 nm

Fig 10

Fig 11

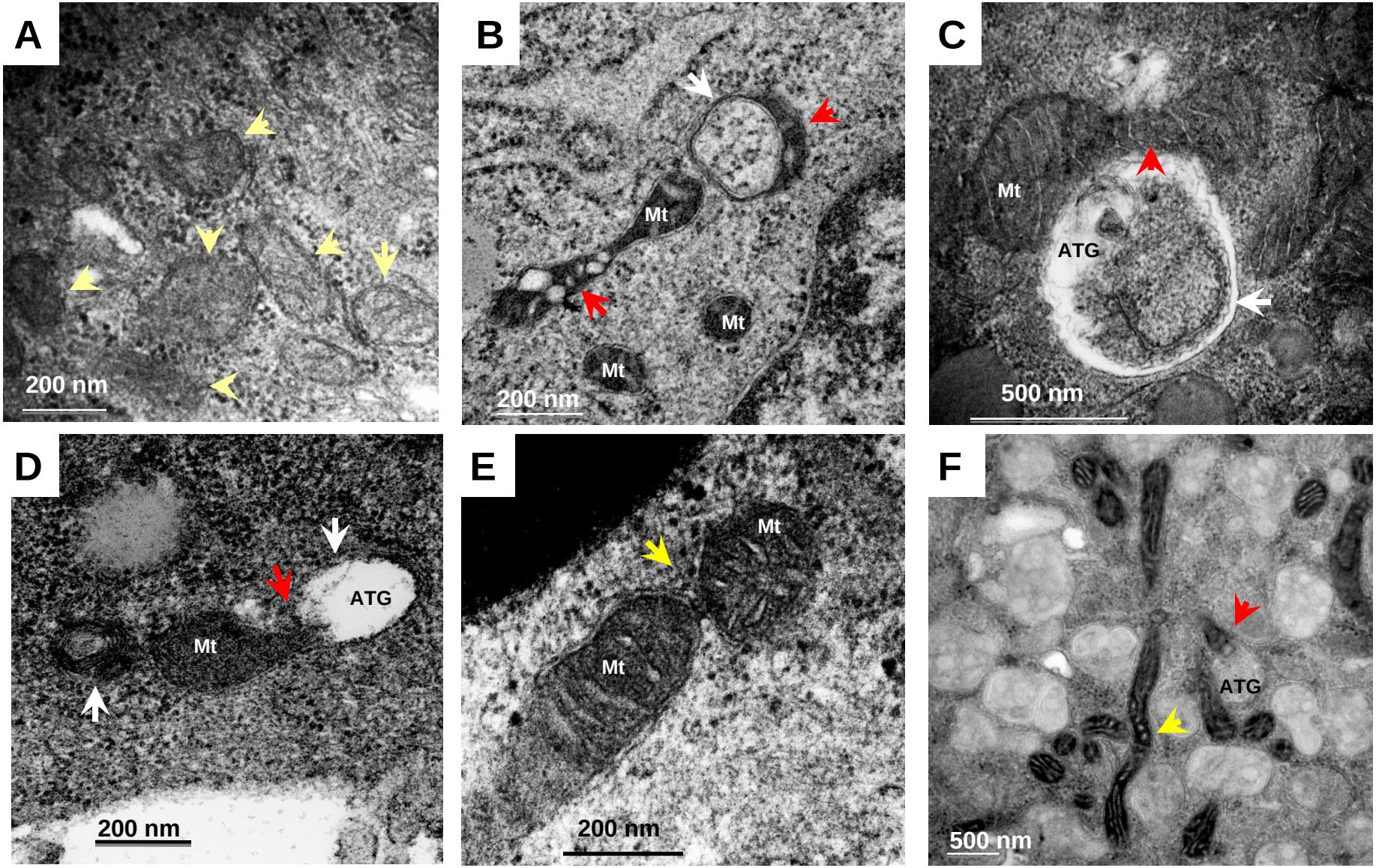
A
200 nm
B
Mt
Mt
Mt
200 nm
C
Mt
ATG
500 nm
D
ATG
Mt
200 nm
E
Mt
Mt
200 nm
F
ATG
500 nm

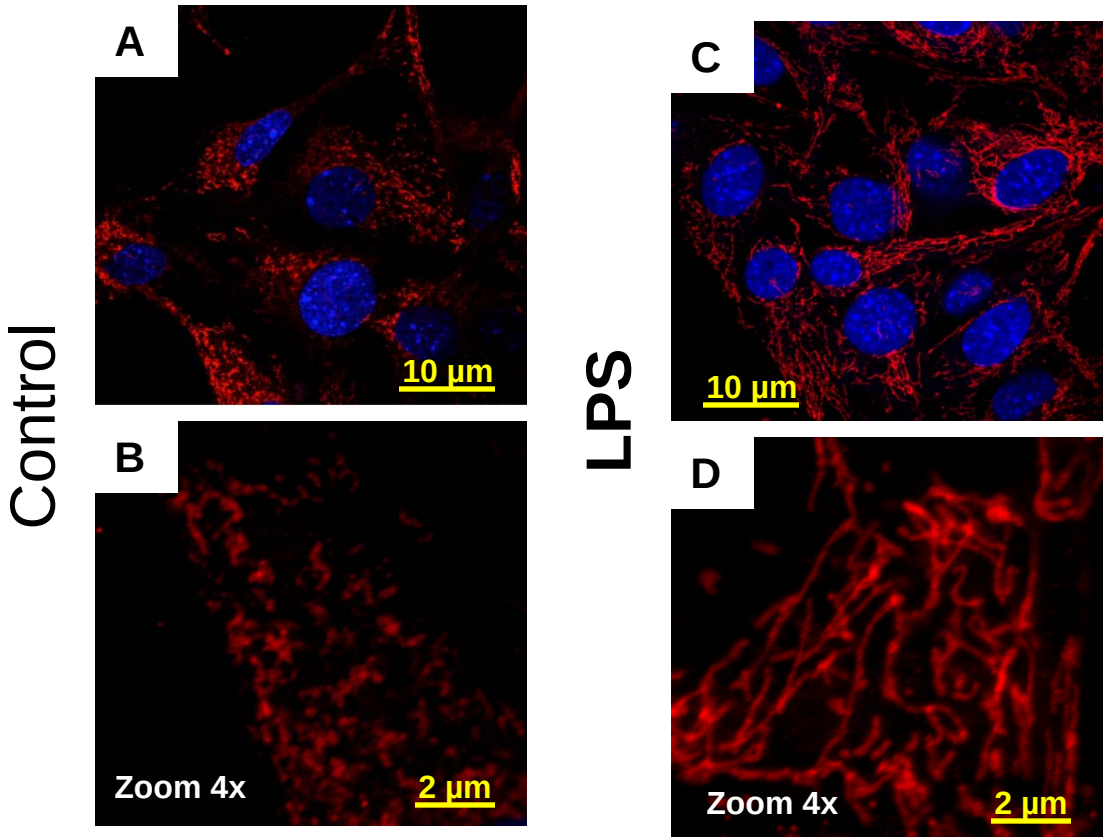

Fig 12